Insights into the promotion with Ru of Co/TiO_2 Fischer-Tropsch catalysts: An in situ spectroscopic study

Francine Bertella[a,b], Christian W. Lopes[a,b], Alexandre C. Foucher[d], Giovanni Agostini[c], Patricia Concepción[a], Eric A. Stach[d], Agustín Martínez[a,*]

[a] *Instituto de Tecnología Química, Universitat Politècnica de València - Consejo Superior de Investigaciones Científicas (UPV-CSIC), Avda. de los Naranjos s/n, 46022 Valencia, Spain.*

[b] *Institute of Chemistry, Universidade Federal do Rio Grande do Sul – UFRGS, Av. Bento Gonçalves, 9500, P.O. Box 15003, 91501-970 Porto Alegre, RS, Brazil.*

[c] *CELLS – ALBA Synchrotron Radiation Facility, Carrer de la Llum 2-26, 08290 Cerdanyola del Vallès, Barcelona, Spain.*

[d] *Department of Materials Science and Engineering, University of Pennsylvania, Philadelphia, Pennsylvania 19104, United States.*

* Corresponding author: amart@itq.upv.es (A. Martínez)

Abstract

Although ruthenium is a common promoter for cobalt-based Fischer-Tropsch synthesis (FTS) catalysts, the origin of Ru promotion and promoter concentration effects remains controversial. In order to gain fundamental understanding of the Ru promotion effects, we herein performed an in situ spectroscopic study by XAS, FTIR, and XPS-Auger of *working* Co/TiO_2 catalysts (ca. 12 wt% Co, pure anatase TiO_2 phase) promoted with different amounts of Ru (0.1 – 1.2 wt%). At typical FTS conditions (220 °C, 20 bar, H_2/CO= 2), the activity in terms of both metal-time-yield (MTY) and TOF was maximized for the catalysts promoted with 0.1 – 0.2 wt% Ru, for which most of Ru was alloyed with Co in bimetallic nanoparticles. The analysis of Auger electrons evidenced that the lower (apparent) TOF of accessible Co^0 sites in the absence of Ru and at Ru concentrations beyond 0.2 wt% is bridged to the development, under reaction conditions, of FTS-inactive cobalt carbide (CoC_x) and cobalt oxide (CoO_x) patches, respectively, at the outermost surface of cobalt crystallites.

Keywords: Fischer-Tropsch synthesis; cobalt catalyst; ruthenium promotion; TiO_2 support; in situ XAS, FTIR, and XPS-Auger spectroscopy.

1. Introduction

Cobalt catalysts supported on porous inorganic oxides like SiO_2, Al_2O_3, and TiO_2 are industrially employed for the production of ultra-clean liquid fuels from syngas in low-temperature Fischer-Tropsch synthesis (FTS) processes [1]. Irrespective of the support, noble metal promoters (e.g. Re, Ru, Pt, Pd, and Ag) are typically added in small quantities to the cobalt catalyst formulation as a means to lower the reduction temperature of cobalt oxides. The improved Co reducibility in noble metal-promoted catalysts is usually ascribed to the supply of H_2 species spilt-over from the more reducible noble metal to nearby Co oxides and/or to the intimate contact between promoter and Co atoms in bimetallic nanoparticles [1-4]. Besides reducibility, the promotion with noble metals often improves the dispersion of the supported Co crystallites [5-8], although marginal variations in Co dispersion are reported in some cases [3, 9-11]. The improvement in Co dispersion is generally related to the noble metal-assisted reduction of small Co oxide species interacting strongly with the support [12] and/or to an increase in the concentration of Co oxide nucleation sites during decomposition of the cobalt precursor resulting in smaller crystallites [5]. Due to the enhancement in Co reducibility and/or dispersion, noble metal-promoted catalysts typically exhibit larger metallic Co surface areas and, consequently, higher FTS reaction rates and C_{5+} selectivities compared to their unpromoted counterparts. Although in most cases the increase in FTS rate upon noble metal promotion apparently occurs without a significant change in the intrinsic reactivity (i.e., TOF) of the exposed Co^0 atoms [5, 7-8, 13], a decreased TOF was found for noble metals exhibiting high hydrogenation activity such as Pt and Pd [6, 13]. Conversely, other studies showed an increase in TOF upon promotion of Co/SiO_2 with Ru [6, 14] and of Co/TiO_2 with Ru, Re, Pt, or Ag [15]. Particularly remarkable is the 3-fold increase in TOF reported in an early work by Iglesia and co-workers upon promotion of Co/TiO_2 (11.6 wt% Co) with small concentrations of Ru (Ru/Co atomic ratios < 0.008), without apparent changes in Co dispersion [9]. However, the fact that the addition of Ru did not alter activation energies and reaction kinetics led the authors to suggest that the enhanced activity likely results from a higher density of active Co^0 sites during catalysis in presence of Ru rather than from a real change in their TOF. Moreover, an increased C_{5+} selectivity was also observed for the Ru-promoted Co/TiO_2 catalysts, which was ascribed to their higher Co^0 site density during steady-state FTS promoting the re-adsorption of α-olefins and, thereby, the further growth of hydrocarbon chains. The Ru promotion effect was ascribed to a synergic effect between Ru and Co atoms in bimetallic nanoparticles, according to which Ru atoms at the surface of Co crystallites facilitate the removal of surface carbon and oxygen species preventing premature deactivation of the catalyst during the

initial stages of the FTS reaction [9]. In a later work, Hong and co-workers [16] also attributed the increase in activity observed upon addition of 0.2 wt% Ru to a Co/SiO_2 (10 wt% Co) catalyst to the formation of bimetallic Co-Ru particles in which, according to in situ XAS measurements, Ru was embedded as individual atoms or small clusters.

Although the concentration of promoter is critical to achieving optimal FTS performance of the Co-based catalysts, systematic studies addressing promoter concentration effects are scarce and somewhat controversial. For instance, for Ru-promoted Co catalysts (20 wt% Co) supported on the ordered mesoporous silica SBA-15, a progressive increase in CO conversion and C_{5+} selectivity was observed with raising the Ru concentration from 0.1 up to 5 wt% [17]. On the other hand, the CO conversion over Ru-Co/γ-Al_2O_3 catalysts (15 wt% Co) prepared by co-impregnation displayed a maximum at 0.3 wt% Ru (Ru/Co = 0.012 at.) without practically affecting C_{5+} selectivity [18]. Differently, a maximum CO conversion was achieved at 0.05 wt% Ru in Ru-Co/γ-Al_2O_3 catalysts (5 wt% Co, Ru/Co = 0.006 at.) obtained by impregnation of pre-synthesized colloidal $CoRuO_x$ nanoparticles [19]. In this case, the C_{5+} selectivity gradually increased with Ru loading in the studied range of 0.025 - 0.1 wt%. In both of these studies, the decrease in activity above the optimum Ru concentration was related to segregation of Ru from Co oxide nanoparticles resulting in a less efficient promotion [18-19]. Yet, in another study using co-impregnated Ru-Co/γ-Al_2O_3 catalysts with 20 wt% Co and Ru loadings of 0.5, 1.0, 1.5, and 2.0 wt%, the CO conversion reached its maximum at 1.0 wt% Ru (Ru/Co = 0.029 at.) with almost no effect of Ru concentration on C_{5+} selectivity [20]. In that case, however, the drop in activity at Ru contents beyond 1.0 wt% was simply ascribed to a lower extent of Co reduction. While most of the previous works addressing promoter concentration effects focused on SiO_2- and Al_2O_3-supported Co catalysts, the influence of this parameter in catalysts supported on TiO_2 was seldom investigated. In this regard, Eschermann et al. found distinct concentration effects in Co/TiO_2 (~ 9 wt% Co) depending on the nature of the noble metal promoter (i.e., Ag, Pt, Ru, Re) [15]. The largest promoter concentration effect was found for Ru, for which both CTY and TOF exhibited a maximum at an intermediate loading of 0.10 wt%, while the C_{5+} selectivity steadily raised with the Ru content (from 0.05 to 0.18 wt%). Concurring with the earlier results reported by Iglesia and co-workers [9], the Co/TiO_2 catalyst promoted with 0.10 wt% Ru (Ru/Co= 0.07 at.) displayed about 3 times higher TOF than the unpromoted one [15]. The reasons why different noble metals lead to distinct promoter concentration effects remained unclear, although the possibility that both the nature and concentration of promoter influenced the extent to which the SMSI (strong metal-support

interaction) effect occurred (and thereby the catalytic properties) in the studied promoted Co/TiO_2 catalysts was not dismissed.

Considering the above, in this work we present a thorough in situ spectroscopic study (XAS, FTIR, XPS-Auger) with the aim of gaining insights into the genesis of Ru promotion and Ru concentration effects on the catalytic performance of high surface area Co/TiO_2-anatase catalysts for FTS at industrially relevant conditions (220 °C, 20 bar).

2. Experimental

2.1. Synthesis of TiO_2-anatase support

The TiO_2 support comprised of pure anatase was synthesized hydrothermally using titanium (IV) butoxide (97%, Aldrich) as precursor in the presence of acetic acid (99.5%, Aldrich). The procedure involved the dropwise addition, at room temperature and under magnetic stirring, of 9.6 cm^3 of the titanium alkoxide precursor to 28 cm^3 of an acetic acid solution (1.5 M). The resulting gel was subsequently transferred to a Teflon-lined stainless steel autoclave (200 cm^3 capacity) and submitted to hydrothermal treatment for 24 h in an oven at 120 °C. Next, the produced solid was separated by centrifugation and extensively washed through repeated (5 times) re-dispersion in ethanol and centrifugation. Finally, the support precursor was dried overnight in an oven heated at 60 °C and then calcined at 400 °C for 4 h (heating rate of 1 °C /min) under flowing air.

2.2. Preparation of $CoRu/TiO_2$ catalysts

Cobalt catalysts promoted with variable amounts of Ru were prepared by incipient wetness co-impregnation of the pre-dried anatase carrier with aqueous solutions of $Co(NO_3)_2{\cdot}6H_2O$ (Aldrich) and $Ru(NO)(NO_3)_3$ (Aldrich) precursors, targeting nominal metal loadings of 10 wt% of Co and 0.25, 0.5, 1.5, and 2.5 wt% of Ru. Following impregnation, the solids were dried overnight at 100 °C and then air-calcined for 3 h at 300 °C. The catalysts were denoted as CoRu*x*/Ti, where *x* stands for the real Ru content determined by ICP-OES. Additionally, two monometallic catalysts were also prepared using the same methodology described above for the bimetallic samples: a Co/TiO_2 (10 wt% Co nominal content) without Ru promoter (labelled as Co/Ti), and a Co-free Ru/TiO_2 sample (labelled as Ru/Ti) with a nominal Ru content of 1.5 wt%.

2.3. Characterization techniques

The materials were characterized by both conventional and advanced techniques. The methods for conventional characterizations, including inductively coupled plasma-optical emission spectrometry (ICP-OES), X-ray powder diffraction (XRD), N_2 adsorption, field emission scanning electron microscopy (FESEM), H_2 temperature-programmed reduction (H_2-TPR), H_2 chemisorption, and scanning transmission electron microscopy (STEM) are described in the Supporting Information. The conditions for the advanced characterizations comprising aberration-corrected STEM (AC-STEM) and in situ spectroscopies (XAS, CO-FTIR, XPS) are reported in this section.

Transmission electron microscopy was performed with an aberration-corrected JEOL NEOARM operating at 200 kV in STEM mode. The samples were diluted in isopropanol and deposited on a lacey carbon film on copper grids. High resolution EDS (Energy Dispersive X-Rays Spectroscopy) maps were obtained with DigitalMicrograph from Gatan with a pixel time of 0.05 seconds for an Ru loading of 1.2 wt% and 0.07 seconds for an Ru loading of 0.2 wt%.

Fourier transform infrared (FTIR) spectra of adsorbed CO and under flowing syngas at FTS conditions (220 °C, 1 bar) were registered at 4 cm^{-1} resolution with a Nexus 8700 FTIR spectrometer equipped with a DTGS detector. In situ measurements were performed in an IR cell, allowing a wide range of temperatures and gas atmospheres, connected to a vacuum and a gas dosing system. Prior measurements, the samples were ex situ reduced in flowing pure H_2 at 400 °C for 10 h and passivated with a flow of diluted O_2 (0.5 vol% in N_2) at room temperature. The ex situ reduced-passivated samples were subsequently pressed into self-supported wafers (ca. 10 mg) and re-reduced in the IR cell at 400 °C for 2 h under H_2 flow (20 cm^3/min), followed by a vacuum treatment at 450 °C for 1 h. For FTIR-CO experiments, the as-reduced samples were cooled down to 25 °C under dynamic vacuum, CO dosed at increasing pressures (1.9 – 30 mbar), and the IR spectra recorded after each dosage. For FTIR experiments under flowing syngas, the temperature was lowered to 60 °C under dynamic vacuum, syngas was then flowed through the IR cell (14 cm^3/min) at atmospheric pressure, and the temperature was increased stepwise up to 220 °C (the FTS reaction temperature). The IR spectra were collected 10 min after reaching the intermediate temperatures of 60, 160, and 200 °C, and after 1 and 4 h of reaction at the final temperature of 220 °C. After recording each spectrum, the samples were let to cool down for 5 min and another spectrum was collected to monitor the re-adsorption of gas phase species. Before concluding the experiments, the cell was evacuated at 220 °C and a final spectrum was measured. The IR spectra were analyzed using the Origin software.

FTIR spectra under flowing syngas were also recorded in the same spectrometer at a pressure of 9 bar using a commercial AABSPEC catalytic cell. Prior measurements, the catalysts, previously reduced and passivated ex situ, were re-reduced in the IR cell under a flow of H_2 at 400 °C for 2 h. Then, the temperature was decreased to 100 °C, and a flow of syngas was established through the cell. Subsequently, the pressure was increased up to 9 bar and the temperature was raised stepwise up to 220 °C. FTIR spectra were collected at 100 °C and 160 °C and, finally, after 4 h at 220 °C.

X-ray photoelectron spectroscopy (XPS) measurements were performed on a SPECS spectrometer provided with a 150-MCD-9 detector using either monochromatic (for Co2p and Ru3d) or non-monochromatic (for C1s) Al K_α (1486.6 eV) X-ray source. XP spectra were acquired at a pressure of 10^{-9} mbar, an analyzer pass energy of 30 eV, and an X-ray power of 200 W. Binding energies were adjusted to the C1s peak of carbon at 284.5 eV. The CASA software was applied for spectral deconvolution. Prior analysis, about 20 mg of sample were reduced at 400 °C for 5 h under flowing H_2 (5 cm^3/min) in a high-pressure catalytic reactor (HPCR) connected to the analysis chamber of the spectrometer under ultra-high vacuum (UHV) to prevent contact of the sample with ambient air. The FTS reaction was carried out in the HPCR at both 1 and 9 bar under flowing syngas (10 cm^3/min) at the temperature of 220 °C for 3 h, while monitoring the reaction products by online mass spectrometry using a Balzer (QMG 220M1, Omnistar) spectrometer running in the multi-ion mode (MID). The reaction was traced by recording the selected mass spectral signals at m/z of 28 (CO), 15 (CH_4), 44 (CO_2), 18 (H_2O), and 2 (H_2).

X-ray absorption spectroscopy (XAS) measurements at the Ru K-edge (22117 eV) were performed at beamline BM23 of the European Synchrotron Radiation Facility (ESRF, Grenoble, France). Monochromatization of the beam and harmonic rejection were performed using, respectively, a Si (111) double crystal and two Pt-coated silicon mirrors. The spectra were acquired in fluorescence mode using a Silicon Drift Detector (SSD) for powered samples placed inside a home-made catalytic cell [21] and previously reduced in situ with H_2 at 400 °C and 1 bar for 3 h. In order to avoid thermal effects on the collected spectra and, consequently, to improve the spectral quality, the temperature was lowered to 100 °C prior data acquisition. Then, syngas (H_2/CO = 2) was flowed through the cell, the temperature raised to the FTS temperature of 220 °C at ambient pressure, and the spectra recorded after 3 h of reaction at this condition.

XAS experiments under flowing syngas at a higher pressure of 7 bars were carried out at the BL22 (CLÆSS) beamline of ALBA synchrotron (Cerdanyolla del Vallès, Spain). A Si (111) double crystal

was used to monochromatize the beam, while harmonic rejection was performed with Rh-coated silicon mirrors. The spectra were collected in fluorescence mode by using a multi-channel fluorescence SSD detector. The catalysts, in the form of pellets with optimized thickness, were placed inside a multipurpose cell allowing in situ experiments. Optimal signal-to-noise ratio and spectral reproducibility were guaranteed by acquiring several scans at each measurement step. Data normalization and extraction of the EXAFS signal were performed using IFEFFIT package [22]. Phase and amplitudes were calculated by FEFF6 code and successfully validated with Ru metal powder. For each sample, the averaged k^3-weighted $\chi(k)$ function was Fourier transformed in a determined $\Delta k = 2.6 – 12.0$ Å^{-1} interval. A co-refinement fit strategy was adopted in order to reduce the number of variables and the correlation between them, fitting all spectra at the same time in different k-weights. This approach was performed once higher errors and fit instability were noticed when regular fits (guessing one Debye-Waller factor and one ΔE_0 for each spectrum) were applied. All fits were done in R-space in the $\Delta R = 1.4 – 3.0$ Å interval using a Hanning window. The amplitude reduction factor (S_0^2) was constrained to that obtained for Ru^0 standard (0.72).

2.4. Fischer-Tropsch synthesis experiments

Fischer-Tropsch synthesis (FTS) experiments were performed in a fixed bed stainless steel reactor loaded with 0.5 g of calcined catalyst (0.25- 0.42 mm pellet size) diluted with the necessary amount of SiC particles (0.6- 0.8 mm) to attain a total bed volume of 6.4 cm^3. Prior reaction, the catalyst precursor was reduced in situ in a flow of pure H_2 at 400 °C (heating rate of 1 °C/min) and 1 bar for 10 h. Next, the temperature was decreased to 100 °C, the H_2 flow replaced by a gas mixture of syngas (H_2/CO molar ratio of 2) and Ar (used as GC standard) in a syngas:Ar volume ratio of 9:1, and the reactor pressure and temperature set at 20 bar and 220 °C (heating rate of 2 °C/min), respectively. During the first 8 h (period 1), the FTS reaction was conducted at a constant gas hourly space velocity (GHSV) of 11.7 $L_{syngas}/(g_{cat}\cdot h)$, enabling the activity of the catalysts to be compared at quasi-differential (< 10%) CO conversions while ensuring a low water partial pressure in the catalytic bed. Afterwards, in order to compare product selectivities at isoconversion, the GHSV was adjusted for each catalyst to attain a constant CO conversion of ca. 10 % in the *pseudo*-steady state and the reaction maintained at this condition during the next 8 h (period 2). Therefore, in total (period 1 + period 2), the FTS experiments lasted about 16 h. Heavy hydrocarbons and water were collected in two consecutive traps maintained at 150 °C and 100 °C, respectively, and 20 bar. The stream leaving the traps was depressurized and regularly analyzed by online gas chromatography in a Varian 450

instrument equipped with thermal conductivity and flame ionization detectors and three columns, as detailed elsewhere [23]. The condensed heavy hydrocarbons were weighted, diluted with CS_2, and analyzed offline in the above GC. Carbon mass balances for the reported experiments were 100 ± 2%. Initial turnover frequencies (TOF_0) were calculated considering the FTS rates extrapolated to zero time on stream (TOS) and the amounts of exposed metal sites derived from H_2 chemisorption measurements. Product selectivities are calculated on a carbon basis.

3. Results and discussion

3.1. Conventional characterization of TiO_2-anatase support and CoRu/TiO_2 catalysts

The properties of the TiO_2-anatase support and the CoRu/TiO_2 catalysts derived from conventional characterization techniques are presented in the Supporting Information. The main outcomes from such characterizations are briefly discussed in this section.

According to XRD (Figure S1) and FESEM (Figure S2), the calcined TiO_2 support comprises 100% pure anatase with rice-like crystallites sizing ca. 10 - 30 nm. The TiO_2-anatase carrier displays a type IV isotherm (Figure S3a), revealing its mesoporous character, with a high BET surface area of 158 m^2/g, a total pore volume of 0.25 cm^3/g, and a unimodal size distribution of mesopores with maximum at 9.1 nm (Figure S3b).

As it can be seen in Table 1, the calcined catalysts show Co loadings of around 12 wt%, as determined by ICP-OES, slightly above the nominal value (10 wt%), while the Ru contents in the Ru-promoted samples (0.1 – 1.2 wt%) are 50 – 60% lower than the nominal ones (0.25 – 2.5 wt%). Such a significant loss of Ru is ascribed to the elimination of volatile RuO_x species generated during the air-calcination treatment catalyzed by Co_3O_4 [16]. The calcined TiO_2-supported Co precursors show the presence of Co_3O_4 as the only Co crystalline phase (Figure S4). Additionally, very low intense X-ray diffractions ascribed to RuO_2 crystallites are detected only for the CoRu1.2/Ti catalyst with the highest Ru loading of 1.2 wt% (see inset in Figure S4). Similar to the pristine anatase support, the Co(Ru)/TiO_2 catalysts exhibit type IV N_2 adsorption isotherms and unimodal pore size distributions with maxima at ca. 9 – 10 nm (Figure S5). Moreover, the small decrease in BET area and pore volume (< 10% when normalized per mass of TiO_2) relative to the pristine support upon incorporation of metals (Table S1) signs for an insignificant blockage of mesopores by the supported metal oxide phases.

As inferred from H_2-TPR measurements (Figure S6), the addition of Ru in concentrations up to 0.7 wt% remarkably lowers the temperature for both Co_3O_4-to-CoO and CoO-to-Co^0 reduction

steps, while a further increment in Ru content from 0.7 to 1.2 wt% does not significantly change the reduction profile. Such differences in cobalt reducibility, however, are substantially attenuated during the reduction treatment with pure H_2 at 400 °C for 10 h, resulting in catalysts that exhibit similarly high degrees of cobalt reduction (DOR) of 88 – 93% (Table 1). However, since part of the H_2 consumed in the H_2-TPR experiments performed in the 400 – 900 °C temperature range to determine the DOR (see Supporting Information) would likely correspond to the partial reduction of the TiO_2 support, the real DOR values in our samples should be even closer to 100%, in line with previous works [24].

Table 1. Metal properties of Co/TiO_2 and $CoRu/TiO_2$ catalysts.

Catalyst	Metal content (wt%)[a]		Ru/Co	DOR[b]	$d(Co^0)_{STEM}$[c]	H_2 uptake[d]
	Co	Ru	atomic ratio	(%)	(nm)	(μmol/g_{cat})
Co/Ti	12.2	-	-	89	12.1	8.9 (85.3)
CoRu0.1/Ti	11.9	0.1	0.005	92	10.4	18.7 (96.7)
CoTi0.2/Ti	11.8	0.2	0.010	88	8.3	17.6 (120.2)
CoRu0.7/Ti	11.4	0.7	0.036	92	8.8	39.1 (109.5)
CoRu1.2/Ti	11.8	1.2	0.059	93	7.8	32.4 (127.9)

[a] Determined by ICP-OES.
[b] DOR: degree of cobalt reduction.
[c] STEM-derived surface average Co^0 particle diameters (D[3,2]).
[d] Values in parenthesis are the theoretical H_2 uptakes calculated from the STEM-derived surface average Co^0 particle sizes assuming spherical particle morphology and 100% cobalt reduction.

An enhanced cobalt dispersion upon promotion of Co/TiO_2 with Ru in concentrations of up to 0.2 wt% is inferred from the decrease in the STEM-derived surface average Co^0 particle size from 12.1 nm for Co/Ti to 8.3 nm for CoRu0.2/Ti (Table 1). According to earlier studies, the improved Co dispersion can be ascribed to the Ru-assisted reduction of hard-to-reduce small Co oxide species more tightly bound to the support surface [12] and/or to the enhanced formation of Co oxide nucleation sites during the metal precursor decomposition in presence of the noble metal promoter [5]. Increasing the Ru content from 0.2 to 1.2 wt%, however, does not significantly alter the mean Co^0 particle size (7.8 – 8.8 nm) and, thus, the average Co dispersion. Representative HAADF-STEM images and the corresponding particle size histograms for the H_2-reduced catalysts are presented in Figure 1. These data clearly show the presence of smaller Co^0 nanoparticles in the Ru-promoted samples, especially in those with higher Ru loading (CoRu0.7/Ti and CoRu1.2/Ti) for which the

relative proportion of nanoparticles sizing less than 6 nm reaches ca. 45% compared to ca. 9% for Co/Ti and CoRu0.1/Ti and 24% for CoRu0.2/Ti. Additionally, for the catalysts promoted with 0.7 and 1.2 wt% Ru, EDS mapping reveals the presence of Ru-rich regions (Figure S7), suggesting the formation of agglomerates of small Ru^0 crystallites at high promoter contents.

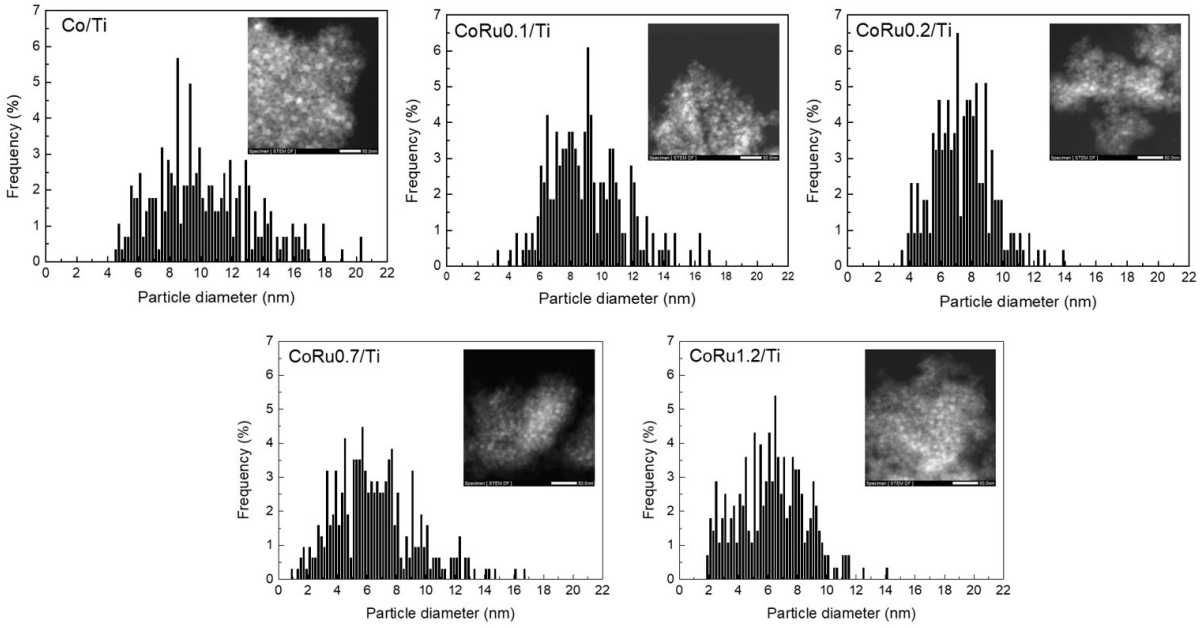

Figure 1. Representative HAADF-STEM micrographs (insets) and corresponding particle size histograms for H_2-reduced and passivated catalysts.

On the other hand, hydrogen chemisorption measurements on the reduced catalysts show about two- and four-fold increases in H_2 uptake (i.e., in the amount of exposed metal sites) upon promotion of Co/TiO_2 with 0.1 – 0.2 and 0.7 - 1.2 wt% Ru, respectively (Table 1). The higher H_2 uptakes displayed by the Ru-promoted catalysts can be ascribed to the improved Co^0 dispersion and, especially at high Ru contents, to the additional chemisorption of H_2 on accessible metallic Ru atoms. Among the catalysts, the unpromoted one (Co/Ti) displays the largest difference between the experimental H_2 uptake and the theoretical value calculated from the STEM-derived Co^0 particle size, evidencing a more pronounced SMSI effect in this catalyst after H_2 reduction at 400 °C in comparison to the Ru-promoted ones. This is supported by the much lower intensity of the IR bands of surface Co carbonyls as titrated by room temperature CO-FTIR spectroscopy (Figure S8). Moreover, the decrease in H_2 uptake at the highest Ru content can be linked to the formation of

larger Ru^0 crystallites, as detected by XRD (Figure S4), as well as to a somewhat more extended SMSI effect in CoRu1.2/Ti, as concluded from CO-FTIR (Figure S8).

As discussed beforehand, some authors attributed the enhanced FTS activity of Co catalysts promoted with Ru to a synergistic effect between Co and Ru atoms in intimate contact within bimetallic particles [9, 16]. Here, the local and electronic structure of Ru species in the H_2-reduced $CoRu/TiO_2$ catalysts was assessed by means of XAS and XPS spectroscopies. The results of these characterizations are discussed in the next section.

3.2. Characterization of Ru species in as-reduced CoRux/Ti catalysts

3.2.1. X-ray absorption spectroscopy (XAS)

The Ru electronic structure in the catalysts reduced in situ under flowing H_2 at 400 °C for 3 h was studied by XAS on the Ru K-edge. As shown in Figure S9, the absorption edge in the normalized XANES spectra for the as-reduced Ru-promoted catalysts matches well that of the reference Ru metal (22117 eV), evidencing the metallic character of Ru species in the former. Interestingly, the oscillations for CoRu0.2/Ti are shifted by ca. 5 eV with respect to those of CoRu0.7/Ti and CoRu1.2/Ti, which suggests a different Ru local order for catalysts promoted with low (0.2 wt%) and high (0.7 – 1.2 wt%) Ru contents.

A more in-depth analysis was obtained by EXAFS through the analysis of the χ(k) functions (Figure 2a) and the respective |FT| spectra (Figure 2b) of the as-reduced catalysts and the reference Ru metal sample. The quantitative results derived from the analysis of the EXAFS data are compiled in Table S2. In Figure 2a, the oscillations at low k-values (2 to 8 $Å^{-1}$) of the catalyst promoted with 0.2 wt% Ru are in antiphase (first two oscillations at, respectively, 3.62 and 5.21 $Å^{-1}$) in comparison to those of the reference Ru^0 sample (first three oscillations with maxima at 3.32, 4.69, and 5.87 $Å^{-1}$, respectively). However, at higher k-values, this catalyst displays oscillations that, although less intense, resemble those of Ru metal. On the other hand, the CoRu0.7/Ti and CoRu1.2/Ti samples show an intermediate behavior between the reference Ru^0 and the CoRu0.2/Ti catalyst at low k-values, pointing out to two distinct local arrangements for Ru atoms in the high-loaded catalysts.

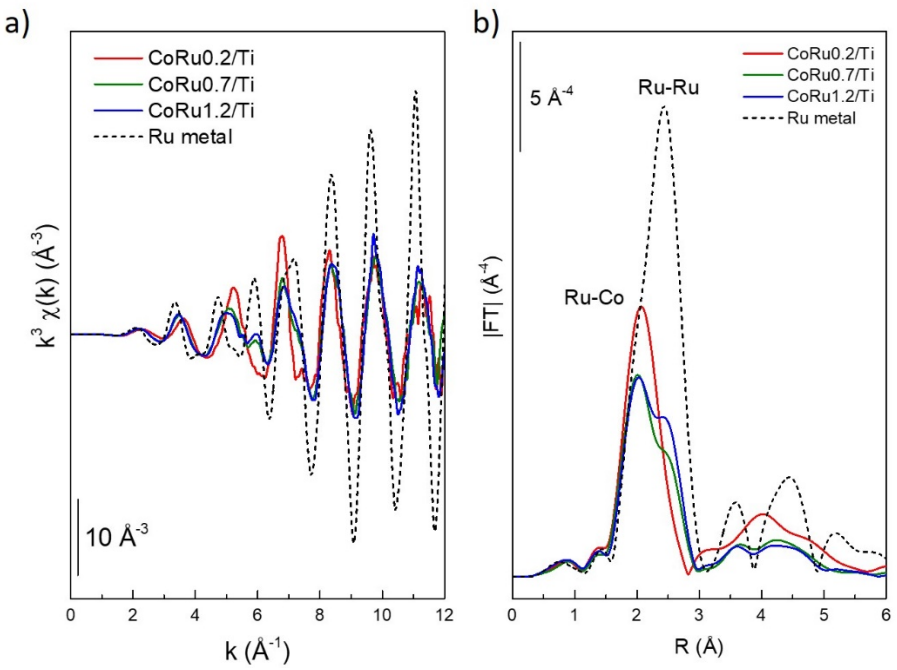

Figure 2. k^3-weighted EXAFS signals (a) and respective moduli of Fourier transform (b) of as-reduced CoRu*x*/TiO_2 catalysts and reference Ru metal.

Differences in the distance and coordination of Ru atoms at low and high Ru loadings are clearly evidenced by analyzing the Fourier transformed EXAFS spectra (Figure 2b). The first shell of CoRu0.2/Ti features a single peak at 2.1 Å (not corrected in phase) related to Ru-Co bonds, resulting in an average coordination number (N_{Ru-Co}) of 8.3 ± 0.8 with neighbors located at a distance of 2.50 Å (Table S2) [9]. This distance is significantly shorter than that of Ru metal (2.67 Å) and very close to the Co-Co distance in metallic Co particles (2.49 Å), which reinforces the formation of a Ru-Co alloy phase. The results in Table S2 also evidence a decrease in the coordination number of alloyed Ru species (N_{Ru-Co}) from 8.3 to 4.4 when increasing the Ru content from 0.2 to 1.2 wt%. This trend could be accounted for by a decrease in the size of nanoparticles (Figure 1) and a Ru-enrichment at the nanoparticle surface with the raise in Ru loading beyond 0.2 wt%, as will be shown in section 3.6 based on XPS. On the other hand, the catalysts promoted with 0.7 and 1.2 wt% Ru exhibit, additionally, a shoulder at a longer distance of 2.4 Å (not corrected in phase) that matches the Ru-Ru distance in monometallic Ru species. This indicates that at low concentrations Ru atoms are mainly alloyed with Co (Co-Ru) and that both alloyed (Co-Ru) and monometallic (Ru-Ru) Ru species coexist at high Ru contents. Nevertheless, a minor contribution of monometallic Ru species in the low-loaded CoRu0.2/Ti catalyst may be inferred from the asymmetry in the right-tail end of the first

shell peak of its EXAFS spectrum (Figure 2b) which, according to their low coordination number (N_{Ru-Ru} = 1.6 ± 0.5, Table S2), should correspond to small Ru^0 clusters. In agreement with STEM-EDS mapping (Figure S7), the decrease in the average Ru-Co coordination number along with the concomitant increase in Ru-Ru coordination number also signs for a higher contribution of segregated metallic Ru species as the Ru loading increases from 0.7 to 1.2 wt% (Table S2). From the Ru-Ru average coordination numbers, an average size for the Ru^0 clusters of 0.8 – 0.9 nm for CoRu0.7/Ti and of 0.9 – 1.0 nm for CoRu1.2/Ti is estimated by assuming a cubo-octahedral morphology, a narrow Ru size distribution, and that all Ru atoms are involved in monometallic Ru-Ru species [25]. However, the similarity of the XANES spectra (preventing a linear correlation approach) and the different Ru contents of CoRu0.7/Ti and CoRu1.2/Ti samples hinder a fair estimation of the fraction of Ru atoms involved in either monometallic or bimetallic (Co-Ru) species by this technique. This will be addressed in the next section based on XPS data.

3.2.2. X-ray photoelectron spectroscopy (XPS)

The analysis of the $Ru3d_{5/2}$ XPS spectra for the H_2-reduced Ru-promoted catalysts revealed two components at about 279.6 eV and 280.5 eV (Figure S10) assigned to Ru-Ru [26] and Ru-Co species [27], respectively. Deconvolution of the $Ru3d_{5/2}$ peak was applied to estimate the amount of surface Ru species involved in monometallic (Ru-Ru) and bimetallic (Ru-Co) particles, assuming that practically all Ru atoms in the bimetallic nanoparticles (sizing, in average, ca. 8 nm) are detected by XPS (penetration depth ~ 6 nm). Ru speciation could not be estimated for the catalyst promoted with the lowest amount of Ru (0.1 wt%) due to a too low signal-to-noise ratio. As shown in Figure 3, about 55% of the surface Ru atoms (10.7 $\mu mol/g_{cat}$) are associated to bimetallic (Ru-Co) species and the remaining 45% (9.1 $\mu mol/g_{cat}$) to monometallic (Ru-Ru) particles in the catalyst promoted with 0.2 wt% Ru.

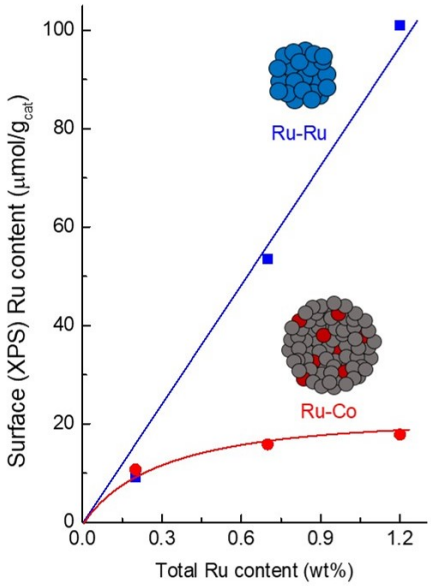

Figure 3. Concentration of Ru species in monometallic (Ru-Ru) and bimetallic (Ru-Co) particles as a function of Ru content in as-reduced CoRu*x*/Ti catalysts estimated from XPS Ru3d$_{5/2}$ peak deconvolutions. Lines are provided as a guide to the eyes.

According to XPS, the concentration of Ru species in monometallic Ru^0 particles raises almost linearly from 9.1 to 101 μmol/g_{cat} with Ru loading. Distinctly, the amount of Ru in bimetallic particles increases significantly (from 10.7 to 15.8 μmol/g_{cat}) with the increment in Ru content from 0.2 to 0.7 wt% and then smoothly (from 15.8 to 17.8 μmol/g_{cat}) with the further increase in Ru content up to 1.2 wt%. As seen in Figure 3, the concentration of Ru in bimetallic particles tends towards a plateau at high Ru loadings that would correspond to the maximum amount of Ru allowed in the Co-Ru alloy.

3.2.3. Aberration-corrected electron microscopy (AC-STEM) and EDS mapping

To clarify the co-existence of cobalt and ruthenium atoms in the same particle and/or the presence of segregated phases we have combined high-resolution AC-STEM imaging and EDS mapping of Co and Ru to further characterize the samples. At low ruthenium loading (sample CoRu0.2/Ti), the EDS map shows some Ru signal (red circle) overlapped with the Co signal (Figure 4a), indicating that they are co-located. However, in other regions the Ru and Co appear segregated. These results are consistent with the above XPS analysis, which indicated the presence of both monometallic (Ru-Ru) and bimetallic (Ru-Co) particles in the low-loaded catalyst (Figure 3). The

previously discussed XAS and XPS results and STEM-EDS mapping (Figure S7) clearly showed an increase for segregated metallic Ru species at promoter concentrations above 0.2 wt%. High-resolution AC-STEM analysis, in turn, provides a direct evidence for part of Ru being closely associated with Co at high Ru loadings. This is indicated by the overlapping of EDS signals of Co and Ru (Figure 4b) and the EDS line scan analysis showing an homogeneous distribution of Co and Ru for both large and small particles (Figure 4c) in the CoRu1.2/Ti catalyst. Therefore, high-resolution AC-STEM and EDS mapping unambiguously confirm that, besides segregated species, Ru atoms are also incorporated into Co nanoparticles even at high Ru contents, in conformity with the previous XPS and EXAFS results.

a)

b)

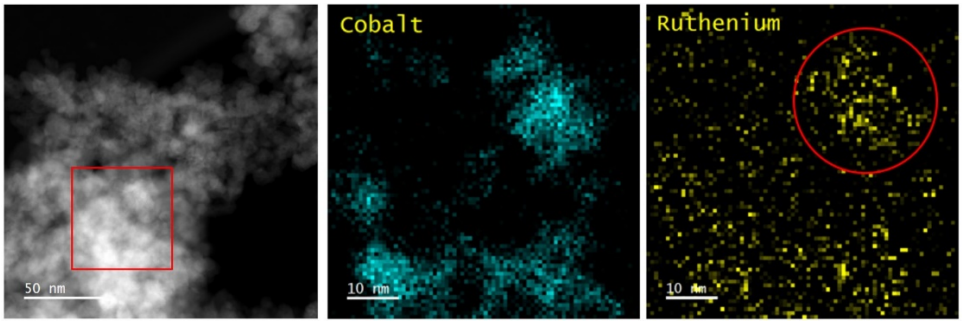

c)

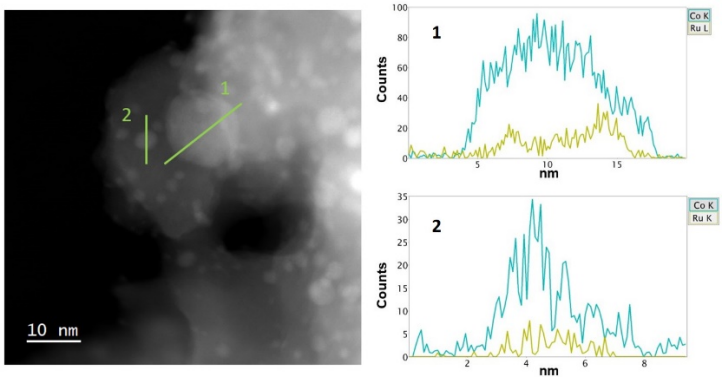

Figure 4. STEM-EDS map of cobalt and ruthenium in the as-reduced and passivated CoRu0.2/Ti (a) and CoRu1.2/Ti (b) catalysts, and EDS line scan analysis of Ru and Co elements in small (line 1) and large (line 2) nanoparticles in the CoRu1.2/Ti sample (c).

3.3. FTS performance of Co/TiO_2 and CoRu/TiO_2 catalysts

As shown in Table 2, all Ru-promoted catalysts present higher initial and *pseudo*-steady state (SS) metal-time yields (MTY) than the Ru-free catalyst. Among the CoRu*x*/Ti samples, those promoted with low amounts of Ru (0.1 – 0.2 wt% Ru) are the most active. In particular, the catalyst containing 0.2 wt% Ru (CoRu0.2/Ti) exhibits the highest activity per total amount of metal, with MTY values that are 4.0 (initial) and 2.6 (SS) times higher than those of Co/Ti. Previous characterization results indicated that, especially at high Ru concentrations, a significant fraction of the Ru species in the as-reduced catalysts exists as agglomerates of small Ru^0 clusters and/or as nanoparticles (as inferred from the presence of XRD-visible RuO_2 particles in the calcined precursor, see inset in Figure S4). Testing of a Co-free Ru/TiO_2 catalyst (0.4 wt% Ru) at the same reaction conditions showed, however, a minor contribution of segregated monometallic Ru^0 species (< 6%) to the initial MTY of CoRu0.7/Ti and CoRu1.2/Ti catalysts (see Supporting Information). We thus conclude that the overall FTS activity of the CoRu*x*/Ti catalysts is mainly dictated by the amount of metal sites (Co+Ru) accessible on the surface of the bimetallic particles.

As observed in Table 2, about a 2-fold increase in TOF_0 is apparent for the catalysts promoted with 0.1 and 0.2 wt% Ru compared to the Ru-free sample. Earlier works also reported 2- to 3-fold higher TOFs for Co/TiO_2 catalysts when promoted with Ru in low concentrations (≤ 0.2 wt%) [9, 15]. For Co/TiO_2 catalysts promoted with Ag, the enhancement in activity with respect to the unpromoted counterpart was ascribed to an increase in the proportion of *hcp*-Co^0 species [15], which were shown to exhibit a higher TOF than *fcc*-Co^0 [28-29]. This explanation, however, appears unlikely in our case since, according to in situ H_2-XRD measurements (Figure S11), both as-reduced Co/Ti and CoRu0.2/Ti catalysts exhibit the same cobalt microstructure, with *hcp*-Co^0 as the main cobalt crystal phase. Both MTYs and initial TOFs sharply raise with increasing the Ru content from 0 to 0.1 – 0.2 wt% and then progressively decline with the further increase in Ru content from 0.2 to 1.2 wt%. It is worth noting that the CoRu*x*/Ti catalysts with Ru contents of 0.7 – 1.2 wt% present initial TOFs ($3.2 \cdot 10^{-2} – 3.5 \cdot 10^{-2}$ s^{-1}) inferior to that of the unpromoted sample ($4.6 \cdot 10^{-2}$ s^{-1}). According to the STEM results discussed before, the samples with higher Ru loading (0.7 – 1.2 wt%) contained a larger proportion of Co^0 nanoparticles sizing less than 6 nm, the critical size below which a lower TOF for

surface Co^0 sites has been reported [30-31]. Therefore, it seems reasonable that the much higher proportion of sub-6 nm Co^0 nanoparticles in the CoRu0.7/Ti and CoRu1.2/Ti catalysts is a factor contributing to their lower initial TOF compared to CoRu0.1/Ti, CoRu0.2/Ti, and Co/Ti. This, however, does not allow us to explain why Co/Ti, with a lower proportion of such small Co^0 nanoparticles, exhibits lower TOF_0 than the catalysts promoted with low amounts of Ru (0.1 – 0.2 wt%).

Table 2. Activity and hydrocarbon selectivity of Co/Ti and CoRu*x*/Ti catalysts for Fischer-Tropsch synthesis at T= 220 °C, P= 20 bar, and H_2/CO = 2 mol/mol.

Catalyst	MTY·10^3 (mol_{CO}/g_{metal}·h)		TOF_0·10^2	Selectivity (%C)[b]		
	Initial[a]	SS[b]	(s^{-1})	C_1	C_2-C_4	C_{5+}
Co/Ti	24.3	21.4	4.6	16.9	32.3	50.8
CoRu0.1/Ti	91.4	52.5	8.1	15.6	28.0	56.4
CoRu0.2/Ti	98.3	55.7	9.3	16.0	27.2	56.8
CoRu0.7/Ti	82.3	39.8	3.5	18.0	29.9	52.1
CoRu1.2/Ti	57.0	32.1	3.2	16.4	27.6	56.0

[a] Extrapolated to TOS = 0.
[b] *Pseudo*-steady state values after adjusting GHSV for each catalyst to attain a CO conversion of ca. 10%.

As shown in Table 2, the addition of Ru enhances the selectivity to the desired C_{5+} hydrocarbon fraction from 50.8 % to 52.1 – 56.8% (depending on Ru content), in agreement with earlier studies [3, 8-9, 19]. This trend is consistent with the respective ASF distributions of hydrocarbons evidencing higher values of the chain growth probability parameter α for the catalysts promoted with Ru (α = 0.75 – 0.78) compared with the unpromoted Co/Ti sample (α = 0.73), as shown in Figure S12 of Supporting Information. Conversely, the selectivity to the C_2-C_4 fraction slightly drops from 32.3% to 27.2 – 29.9 % upon promotion with Ru, whereas all catalysts exhibit an alike selectivity to methane in the range of 15.6 – 18.0% (Table 2). In an earlier study by Iglesia et al. [9], the increase in C_{5+} selectivity observed upon promotion of a Co/TiO_2 catalyst (ca. 12 wt% Co) with 0.14 wt% Ru was ascribed to an enhanced re-adsorption of α-olefins resulting in longer hydrocarbon chains and lower olefin-to-paraffin (O/P) ratios of the formed FTS products. In the present study, however, the Ru-promoted catalysts display, at a constant CO conversion of ca. 10%, remarkably higher O/P ratios for the C_2-C_4 and C_5-C_8 hydrocarbon fractions than the unpromoted catalyst (Figure S13), a trend that does not support the α-olefin re-adsorption mechanism as the likely cause of the enhanced C_{5+}

selectivity exhibited by the CoRu*x*/Ti catalysts. This apparent discrepancy probably stems from differences in the properties of the TiO_2 support employed in our study and in that by Iglesia and co-workers. Thus, while we used a home-synthesized 100% pure anatase TiO_2 with high surface area (158 m^2/g), a low surface area (35 m^2/g) TiO_2 consisting of 70% rutile was employed in the work by Iglesia et al. [9]. The much lower surface area of the TiO_2 carrier in the later study would lead, at an equivalent Co loading of ca. 12 wt%, to a much higher Co site density and, consequently, to more severe pore transport restrictions favoring α-olefin re-adsorption events. Additionally, the fact that, as shown in our previous studies, the SMSI effect occurs to a lower extent in rutile compared to anatase [32] and with decreasing the TiO_2 surface area [33] may also contribute to a larger Co site density (promoting α-olefin re-adsorption and further chain growth) during FTS in the CoRu/TiO_2 catalysts studied by Iglesia and co-workers.

Previous surface science and theoretical studies on model Co catalysts showed that, while CO dissociation is more favored on defected Co^0 sites (e.g., in steps, corners, etc.), C-C chain growth leading to higher hydrocarbons requires relatively large ensembles of Co^0 atoms on the terraces of Co^0 crystallites [34-35]. Considering this, a reasonable hypothesis to explain the lower C_{5+} selectivity of Co/Ti compared to CoRu*x*/Ti catalysts could be a reduction in the size of the Co^0 ensembles on the terraces of Co nanoparticles due to a more extended SMSI decoration effect in the unpromoted sample, as inferred from the FTIR-CO results discussed previously (Figure S8).

Finally, it is worth noting that the hydrocarbon selectivity is barely influenced by the Ru content in Ru-promoted catalysts (Table 2). Since, for these catalysts, large differences in the extension of the SMSI effect were not evidenced, we suggest that the alike hydrocarbon selectivity observed at low (0.1 – 0.2 wt%) and high (0.7 – 1.2 wt%) Ru concentrations originates from the opposing effects of two factors having a marked impact on the ultimate selectivity of Co-based FTS catalysts. On one side, according to the *intrapellet* diffusion-controlled selectivity model developed by Iglesia [36], an enhanced C_{5+} selectivity could be anticipated for the catalysts with high Ru contents presenting comparatively higher values for the diffusion-related structural parameter χ (Table S3) and, hence, a higher resistance to the *intrapellet* diffusion of α-olefins promoting their re-adsorption and participation in chain growth events. This is supported by the somewhat lower olefin-to-paraffin ratios in the hydrocarbon products obtained at Ru contents beyond 0.2 wt% (Figure S13). On the other side, a decreased selectivity of C_{5+} hydrocarbons could be expected at high Ru loadings as these catalysts exhibit a much higher proportion of very small (sub-6 nm) Co^0 nanoparticles (Figure 1), for which an intrinsically higher methane selectivity (in detriment of C_{5+}) has been reported [23, 30].

Since the characterizations discussed in the previous sections cannot fully account for the trends in FTS activity upon promotion of Co/TiO_2 with variable amounts of Ru, the catalysts were additionally characterized under FTS conditions by XAS, FTIR, and XPS spectroscopies with the aim of gaining further insights into the genesis of the observed Ru promotion effects. The results of the in situ spectroscopic characterization are discussed next.

3.4. In situ XAS characterization of CoRu/Ti catalysts

The Ru local environment in the $CoRu/TiO_2$ catalysts with Ru loadings of 0.2 and 1.2 wt% during FTS was investigated by XAS. The EXAFS data after 3 h of reaction at 220 °C and 1 bar are included, besides those for the H_2-reduced samples (recorded at 100 °C), in Table S2. The moduli of Fourier transform (|FT|) for CoRu0.2/Ti and CoRu1.2/Ti catalysts after reduction with H_2 and after FTS reaction are shown in Figure 5. The corresponding fits are presented in Figure S14 (Supporting Information). The spectra for both catalysts during FTS show similar profile but lower amplitude in comparison to those in their as-reduced state, which is mainly attributed to the different thermal effects imposed to EXAFS signal during data acquisition (100 °C for H_2-reduced vs 220 °C after FTS reaction), rather than to a decrease in the coordination numbers. Therefore, a slight change in Ru coordination number under reaction conditions cannot be excluded. On the other hand, a small change in the Ru environment under reaction conditions probably caused by the interaction of Ru with adsorbed surface species (e.g., H^*_{ads}, C^*_{ads}) following CO dissociation is inferred from the elongation of Ru-Co and Ru-Ru distances in these catalysts after FTS (Table S2).

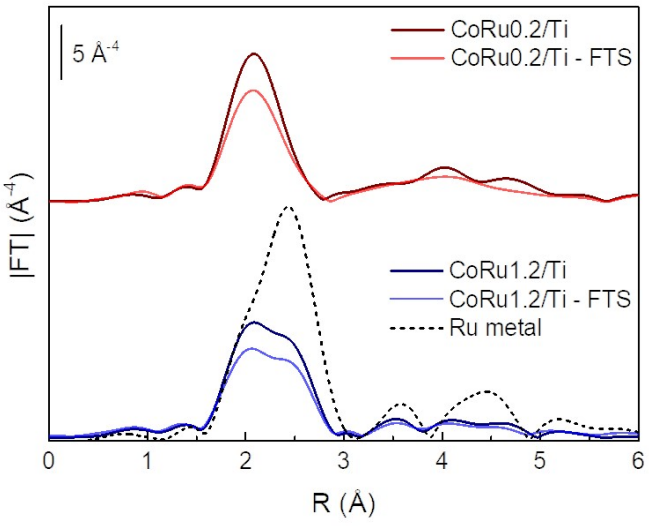

Figure 5. Moduli of Fourier transform of the EXAFS spectra of CoRu0.2/Ti and CoRu1.2/Ti catalysts in their as-reduced state and under FTS conditions (220 °C, 1 bar, 3 h). The spectrum of the reference Ru metal sample is also shown for comparative purposes.

It is worth noting that, for CoRu0.2/Ti after FTS, the features of the higher shells (3 – 5 Å) related to multiple scattering contributions do not resemble those of the as-reduced sample. This behavior could be attributed to a change in the Ru local environment under FTS conditions, as discussed above. The change in higher shells, however, would be less perceptible for the CoRu1.2/Ti catalyst due to its much higher Ru content in comparison with CoRu0.2/Ti. Finally, as seen in Table 2, the small values of R-factors provide evidence for the goodness of fits.

The influence of syngas pressure on the Ru local environment was assessed for the catalysts promoted with 0.2 and 1.2 wt% Ru by performing additional in situ XAS measurements under syngas flow at a pressure of 7 bar and 220 °C (not shown). These experiments, however, did not reveal substantial differences with respect to those performed at atmospheric pressure and, therefore, the general features observed in the later can be taken as representative of the behavior at more realistic FTS pressures.

3.5. Characterization of catalysts by in situ FTIR spectroscopy

FTIR spectroscopy is a very sensitive characterization technique to study the surface of catalysts *at work* as well as, when using CO as reactant, to follow the nature of surface metal species under reaction conditions. Here, we carried out in situ FTIR experiments under flowing syngas at 1 bar and 220 °C to study the evolution of the surface Co species during FTS. Even though FTS reactions are typically carried out at higher pressures of around 20 bar, in situ FTIR characterization at 1 bar of syngas has revealed instrumental in deriving relevant structure-performance correlations for supported Co-based FTS catalysts [23, 37]. Figure 6 depicts the FTIR spectra registered under flowing syngas at 1 bar for the catalysts promoted with 0.2 and 1.2 wt% Ru and for the unpromoted one during the increase of temperature from 60 to 200 °C (spectra 1-3) and after reaction for 1 and 4 h at 220 °C (spectra 4-5). At the temperatures of 200 and 220 °C, the spectra were also recorded after cooling the samples for 5 min (shown as bold lines) in order to monitor the re-adsorption of gas phase species. At the end of the experiment, the catalytic cell was evacuated and a final spectrum was acquired under vacuum at 220 °C (spectrum 6).

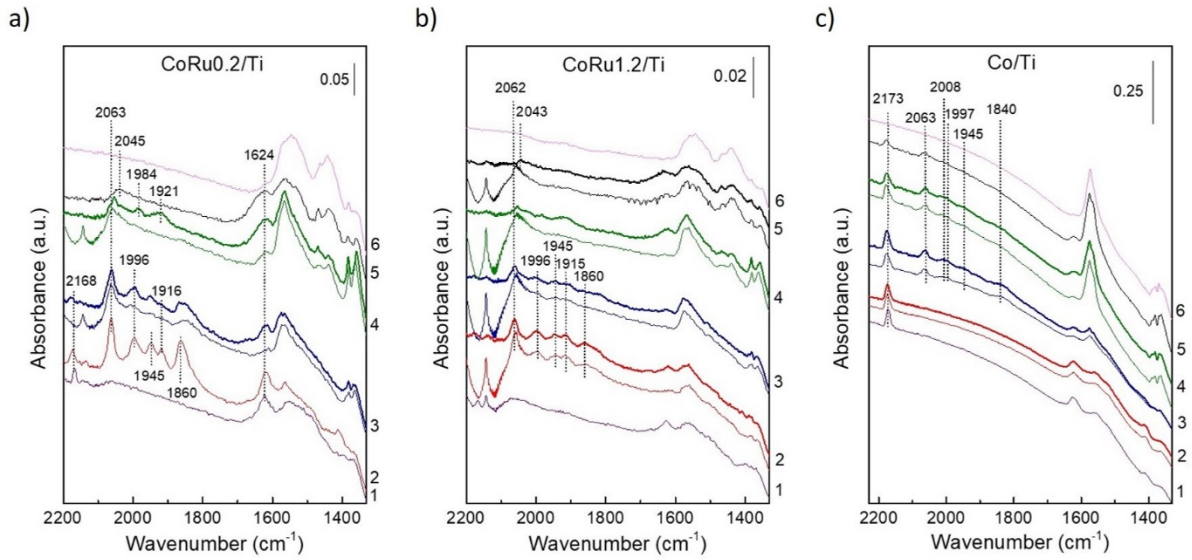

Figure 6. FTIR spectra of CoRu0.2/Ti (a), CoRu1.2/Ti (b), and Co/Ti (c) catalyst under syngas flow (1 bar) at increasing temperature: 60 °C (1), 160 °C (2), 200 °C (3), after 1 h at 220 °C (4), after 4 h at 220 °C (5), and after evacuation at 220 °C (6). Bold lines correspond to the spectra recorded after cooling the samples (see text).

At 60 °C under syngas atmosphere, the CoRu0.2/Ti catalyst (Figure 6, spectrum 1) exhibits low intense IR bands in the 1410-1370 cm^{-1} region related to surface hydrocarbon species (C_xH_y) [38], indicating the occurrence of catalysis already at this low temperature. In the Co-carbonyl region, an IR band at 2168 cm^{-1} due to CO adsorbed on oxidized cobalt species [39] that were not reduced after the in situ re-reduction treatment performed in the IR cell can be seen. The lack of IR bands in the region 2060-1750 cm^{-1} related to metallic cobalt signs for a blockage of the surface Co^0 sites by adsorbed hydrocarbon (C_xH_y) intermediates and probably also by partially reduced TiO_x species migrated from the support (SMSI effect). At the temperature of 160 °C (spectrum 2), intense and well-defined IR bands of Co carbonyls with maxima at 2063, 1996, 1945, 1916, and 1860 cm^{-1} are clearly detected. IR bands at around 2060 cm^{-1} have been indistinctly assigned to CO adsorbed linearly on Co^0 [39], polycarbonyl species ($Co(CO)_x$, x > 1) located at corner sites on the surface of Co particles [6], partially hydrogenated Co(H)-CO species [39], and CO adsorbed on partially charged cobalt atoms ($Co^{\delta+}$) [31]. Furthermore, IR bands in the region of 2000-1750 cm^{-1} have been generally assigned to CO adsorbed at defect sites on the surface of Co^0 nanocrystals as well as to CO adsorbed in a bridged mode on Co^0 [39-40]. In those cases, the corresponding IR bands are expected to exhibit a high thermal stability. However, the species related to the IR bands at 1996, 1945, 1916, and 1860 cm^{-1}

are seen to desorb to the gas phase at 200 °C and decompose leading to new IR bands at 1984 and 1921 cm^{-1} when reaching 220 °C (spectrum 4), signing for a low thermal stability. Differently, the IR band at 2063 cm^{-1} remained visible at increasing temperatures, indicating that it is likely related to more stable linear CO-Co^0 species. Therefore, considering the low thermal stability of these bands, and according to previous works [41-42], we ascribe the low frequency bands (2000-1860 cm^{-1}, Figure 6a, spectra 2 and 3) to polycarbonyls adsorbed on low nuclearity Co^0 clusters. At increasing temperatures, such volatile carbonyl species decompose into linear monocarbonyls leading to new bands at 1984 and 1921 cm^{-1}, as observed in spectrum 4 of Figure 6a. The formation of cobalt polycarbonyls has been shown to depend on the local environment of the surface cobalt atoms [43]. As discussed before, all catalysts in this work experienced the SMSI effect during H_2 reduction at 400 °C. Taking into account that partial reversion of the SMSI state is likely to occur under FTS reaction conditions [44], we suggest a dynamic process by which cobalt polycarbonyls are formed on new unsaturated cobalt sites generated upon removal of TiO_x species from the nanoparticles surface due to their oxidation during reaction by water. Finally, as seen in spectrum 4 of Figure 6a, the intensity of the band at 1624 cm^{-1} of adsorbed water increases and IR bands in the 1590-1350 cm^{-1} region, suggestive of the formation of formate, carboxylate, and C_xH_y species [38, 45-46], develop upon reaching the reaction temperature of 220 °C. These species exhibit a rather weak interaction with the catalyst surface, as inferred from their partial removal upon evacuation of the cell at high temperature (spectrum 6). Furthermore, the fact that the band at 2168 cm^{-1} is no longer detected at 220 °C indicates that the associated oxidized cobalt species previously observed at 60 °C were reduced to Co^0 under FTS conditions. On the other hand, the shift of the IR band of linear CO-Co^0 species from 2063 cm^{-1} to 2045 cm^{-1} observed after 4 h of reaction at 220 °C evidences a surface reconstruction of Co^0 nanoparticles encompassing the formation of new unsaturated (defected) Co^0 sites during FTS [31, 47]. Cobalt atoms at defect sites have been predicted by DFT to be more reactive towards CO dissociation (the kinetically relevant step in FTS) than those on extended facets of the cobalt crystallites [48].

The FTIR-syngas spectra for the catalyst with the highest Ru loading (CoRu1.2/Ti) are presented in Figure 6b. As observed, this catalyst exhibits IR features that closely resemble those of CoRu0.2/Ti discussed beforehand. Hence, in addition of presenting similar IR bands, it also experiences the shift of the main cobalt-carbonyl IR band from 2062 to 2043 cm^{-1} after 4 h of reaction at 220 °C (spectrum 5 in Figure 6b). This behavior indicates that surface reconstruction of

the Co^0 nanoparticles towards more defected planes occurs for the Ru-promoted catalysts under FTS conditions irrespective of the Ru content.

A distinct behavior is observed for the unpromoted Co/Ti catalyst (Figure 6c). While, as the Ru-promoted samples, this catalyst also presents, at 60 °C (spectrum 1), the IR band at 2173 cm^{-1} of oxidized Co species and the features in the 1410-1370 cm^{-1} region of adsorbed C_xH_y intermediates, no obvious changes in the IR bands were noticed upon increasing the temperature up to 160 °C (spectrum 2). At 200 °C, however, the band of linear cobalt carbonyl at 2063 cm^{-1} and the features of cobalt polycarbonyls peaking at 2008, 1997, 1945 and 1840 cm^{-1} are evidenced (spectrum 3), albeit with a lower intensity than in the Ru-containing samples. After exposure of the catalyst to syngas at 220 °C for 1 h (spectrum 4), the polycarbonyl bands vanish while intense bands develop in the region of 1590 – 1350 cm^{-1} related to adsorbed intermediates like formates, carboxylates, and hydrocarbons [38, 45-46]. The later bands remain visible after evacuation of the cell (spectrum 6), indicating that they are firmly held on the catalyst surface. Interestingly, the IR band at 2063 cm^{-1} of linear CO-Co^0 species stays unchanged even after prolonged exposure to syngas at 220 °C (spectrum 5), which evidences the lack of surface reconstruction in the Ru-free catalyst. Both recent theoretical and experimental studies point to a key role of adsorbed C adatoms formed by CO dissociation in promoting surface reconstruction of cobalt crystallites [23, 49]. Therefore, surface reconstruction is expected to be restricted in catalysts exposing a low amount of active surface Co^0 sites (leading to a low surface coverage by dissociated C species), as in Co/Ti experiencing a more extended SMSI effect compared to CoRu*x*/Ti. It is worth noting that the band at 2173 cm^{-1} related to oxidized cobalt species is still observed for Co/Ti during reaction at 220 °C (Figure 6c), underlining the role of Ru species in the promoted catalysts in supplying activated hydrogen species, via spillover, to nearby Co oxide species on the surface of cobalt crystallites. Likewise, the limited hydrogenation capacity in the absence of Ru might also explain the stronger interaction of the hydrocarbon intermediates with the surface of Co/Ti.

Additionally, the Co/Ti, CoRu0.2/Ti, and CoRu1.2/Ti catalysts were characterized by in situ FTIR under flowing syngas at 9 bar. In principle, the use of a higher, more realistic, reaction pressure was expected to enhance the CO conversion rate and, consequently, to intensify the structural changes experienced by the catalysts *at work*, facilitating their investigation by FTIR spectroscopy. Unfortunately, the enhanced reactivity of the catalysts at the higher syngas pressure resulted in a too low intensity of the cobalt carbonyl IR bands under FTS conditions due to an increased amount of adsorbed hydrocarbon intermediates, preventing an effective titration of the surface Co^0 sites by

CO. As an example for this, the temperature-resolved FTIR-CO spectra recorded under flowing syngas at 9 bar for Co/Ti and CoRu0.2/Ti catalysts displaying, respectively, the lowest and highest metal-time yields are shown in Figure S15 of Supporting Information. An additional factor contributing to the attenuated intensity of the IR bands is the small diameter of the IR cell windows that had to be used to withstand the higher reaction pressure. Therefore, in spite of our initial expectations, the FTIR-syngas experiments at 9 bar revealed useless to provide additional information on the catalysts with respect to those performed at ambient pressure.

According to the in situ FTIR study at 1 bar, the lower amount of exposed Co^0 sites as a consequence of a more extensive site blockage by strongly adsorbed intermediates and decorating TiO_x species in Co/Ti would contribute to its lower FTS activity compared to CoRu*x*/Ti (Table 2). However, the contrasting activity of CoRu0.2/Ti *versus* CoRu1.2/Ti cannot be explained based on the nature of cobalt sites exposed during reaction, since both samples showed similar evolution of surface cobalt species during the in situ FTIR experiments. Moreover, the results of the FTIR study can hardly account for the lower TOF_0 of the catalysts promoted with high amounts of Ru (CoRu0.7/Ti and CoRu1.2/Ti) with respect to the Ru-free Co/Ti catalyst (Table 2). As discussed in the next section, we carried out in situ XPS experiments in an attempt to further understand the catalytic behavior of the catalysts under study.

3.6. In situ XPS characterization of Co/Ti and CoRux/Ti catalysts

X-ray photoelectron spectroscopy (XPS) is a highly sensitive surface technique to the chemical environment of the elements under study, particularly when analyzing the Auger peaks. In this work, XP spectra were recorded for the catalysts in their as-reduced state and after in situ FTS reaction at 220 °C and at both 1 and 9 bar. The XPS study at a pressure of 1 bar, however, did not reveal noticeable differences in neither the Co2p nor the Co-AES (Auger) signals for the catalysts in their as-reduced state and after 3 h of FTS reaction, as exemplified in Figure S16 (panels a and b) for the most active CoRu0.2/Ti catalyst. This is attributed to the almost lack of catalysis under these reaction conditions, as supported by the absence of hydrocarbon products in the online MS analysis (not shown). Distinctly, the formation of hydrocarbon products was unambiguously observed by MS for all catalysts in the experiments performed at 9 bar (Figure S17), signing for the occurrence of catalysis at this higher reaction pressure. It is important to highlight that, as seen in Figure S17, the activity ranking of the catalysts in the experiments at 9 bar (CoRu0.1/Ti ≈ CoRu0.2/Ti > CoRu0.7/Ti > CoRu1.2/Ti > Co/Ti) matched well that obtained in the fixed bed reactor at 220 °C and 20 bar (Table

2). Therefore, we can safely assume that, in spite of the pressure gap, the catalyst changes observed in the current in situ XPS study at 9 bar would be representative, at least qualitatively, of those occurring under more realistic conditions.

For all catalysts, an increase in the concentration of adsorbed surface C species was noticed after reaction with syngas compared to that determined for the as-reduced samples (not shown), which further confirms the occurrence of catalysis at the studied conditions. Deconvolution of the C1s XPS peak of the catalysts after FTS reaction (Figure S18) evidences the presence of different surface carbon species, namely aliphatic C-C (284.5 eV), C-O(H) (285.3 eV) [50], oxygenated compounds (288.7 eV) [51], and carbidic carbon (282.5 eV) [52]. This concurs with the nature of the adsorbed species observed in the FTIR-syngas experiments at 1 bar as well as with the results of the in situ XAS study, from which the presence of adsorbed species was suggested based on the elongation of Ru-Ru and Ru-Co bonds during reaction.

The surface atomic ratios for the catalysts in their as-reduced state (H_2) and after reaction with syngas (FTS) are presented in Table 3. The Co/Ti atomic ratios for the H_2-reduced catalysts are consistent with a higher concentration of Co atoms exposed on the surface of the Ru-free catalyst (0.032) in comparison with the catalysts promoted with Ru. Moreover, a decrease in the Co/Ti atomic ratio from 0.030 to 0.020 is evidenced for the Ru-promoted catalysts as the Ru content raises from 0.1 to 1.2 wt% due to the dilution effect at increasing Ru loadings. On the other hand, considering the penetration depth of the X-rays in the XPS analyses (around 6 nm) and the very thin nature of the TiO_x species decorating the Co atoms, establishing a relationship between the extension of the SMSI effect and the surface Co/Ti ratio is not straightforward.

Moreover, the Ru/Ti and Ru/Co atomic ratios in the H_2-reduced catalysts increases from 0.002 to 0.016 and from 0.069 to 0.800, respectively, with the raise in Ru loading from 0.2 to 1.2 wt% (Table 3), as expected. It is worth noting that the atomic Ru/Co ratios determined by XPS are significantly higher than the bulk ratios, the difference being larger at increasing Ru contents (for instance, the surface-to-bulk atomic Ru/Co ratio for the H_2-reduced samples amounts to 6.9, 9.7, and 13.6 for catalysts loaded with 0.2, 0.7, and 1.2 wt% Ru, respectively). This indicates that Ru atoms in CoRu*x*/Ti catalysts preferentially reside at the external surface of the Co crystallites, as also found for Co-Ru/TiO_2 [9] and Co-Ru/SiO_2 [6], and that the surface becomes gradually enriched in Ru at increasing promoter concentrations.

Table 3. Surface atomic ratios derived from XPS for as-reduced catalysts (H_2) and after 3 h of reaction with syngas at 220 °C and 9 bar (FTS).

Catalyst	Co/Ti		Ru/Ti		Ru/Co	
	H_2	FTS	H_2	FTS	H_2	FTS
Co/Ti	0.032	0.035	-	-	-	-
CoRu0.1/Ti	0.030	0.043	bdl[a]		bdl[a]	
CoRu0.2/Ti	0.029	0.037	0.002	0.005	0.069	0.135
CoRu0.7/Ti	0.023	0.025	0.008	0.009	0.348	0.360
CoRu1.2/Ti	0.020	0.020	0.016	0.016	0.800	0.800

[a] Below detection limits.

Interestingly, while for the unpromoted catalyst and those promoted with 0.7 and 1.2 wt% Ru the Co/Ti, Ru/Ti, and Ru/Co atomic ratios remain almost unchanged after reaction, they significantly increase for the catalyst promoted with low amounts of Ru (Table 3), suggesting a higher dynamic behavior of the metal species in the later. Since the lab-scale XPS analyses are not sensitive enough to detect changes in the TiO_x overlayer, especially at low TiO_x coverages, the variations in surface atomic ratios seen for CoRu0.2/Ti might point to morphological changes experienced by the bimetallic Co-Ru nanoparticles, probably induced by the disruption of Co-O-Ti linkages due to the SMSI reversion under reaction conditions.

The asymmetry of the Co^0 XPS peak produced by the presence of two plasmon loss peaks at ca. 3.0 eV and 5.0 eV above the main signal [53] (contributing to the total peak area by, respectively, ca. 11 and 8%) makes fitting of the $Co2p_{3/2}$ signal difficult. In turn, the fact that both plasmon peaks appear at the same binding energy (BE) than Co(OOH) and Co_3O_4 compounds prevents a fair assessment of the presence or absence of oxidic cobalt species. Therefore, we analyzed the Co Auger peaks and determined the modified Auger parameter (α'), which is very sensitive to the chemical state of the analyzed element [54], to characterize the cobalt species in the *working* catalysts by confronting the obtained α' values with those of reference cobalt compounds (Co^0, CoO, Co_3O_4) [55] through the so-called Wagner plot.

The Co LMM Auger peaks of the Ru-free and Ru-promoted samples after FTS are presented in Figure 7a. All catalysts exhibit a main peak with a maximum at kinetic energy (KE) of ca. 774.1 eV, leading to an α' value of ~ 1552 eV that, by comparison with that for the reference samples in the Wagner plot, clearly corresponds to metallic cobalt (Figure 7b). While the Co Auger peak for

CoRu0.2/Ti appears quite symmetric, an asymmetry at lower KE (ca. 772.6 eV) is observed for CoRu0.7/Ti, yielding in this case an α' value of 1550.4 eV. This α' value locates in the Wagner plot close to the line where the reference CoO appears, signing for the presence, besides metallic cobalt, of oxidized surface cobalt species in this catalyst. Moreover, a shoulder at a higher KE of 776.7 eV, equivalent to α' of 1554.4 eV, is detected in the Co LMM Auger spectrum of sample CoRu1.2/Ti (Figure 7a). According to the Wagner plot, this value is similar to that obtained for the reference Co_3O_4 (Figure 7b) which, not only indicates the presence of oxidized surface cobalt species at the highest Ru loading too, but that cobalt in such species is in a higher oxidation state than in CoRu0.7/Ti. Therefore, the analysis of the Co-AES signals through the Wagner plot unambiguously shows the formation of oxide-like Co patches on the outermost surface of the catalysts promoted with 0.7 and 1.2 wt% Ru during FTS, even if cobalt in the bulk of the particles remains essentially metallic.

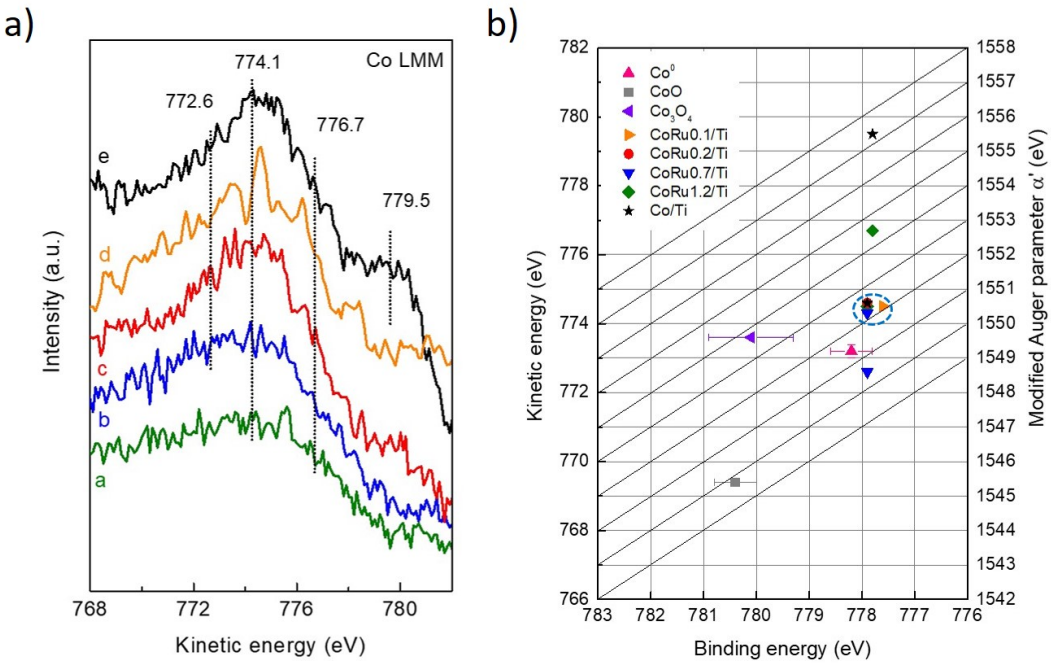

Figure 7. a) Co LMM Auger spectra, and b) Wagner plot for CoRu1.2/Ti (a), CoRu0.7/Ti (b), CoRu0.2/Ti (c), CoRu0.1/Ti (d), and Co/Ti (e) catalysts after FTS reaction at 220 °C and 9 bar for 3 h. Data for reference cobalt compounds (Co^0, CoO, Co_3O_4) are also included in the Wagner plot.

Although, at this point, the origin of formation of oxide-like Co patches on the surface of Co crystallites during FTS at high Ru loadings is uncertain, we hypothesize that this could relate to

electronic interactions between Co and Ru atoms in the bimetallic nanoparticles arising from their different electronegativity. Thus, the higher electronegativity of Ru (2.30) compared to Co (1.88) would induce a partial electron charge transfer from Co^0 to adjacent Ru^0 atoms leaving the former somewhat positively charged, as it has been reported for different bimetallic compositions [56-57]. Moreover, the electron charge transferred between the constituent metallic atoms, and thereby the catalytic performance, shows a strong dependence on the composition of the bimetallic nanoparticle [58-60]. Considering this, the electronic effect in our CoRu*x*/Ti catalysts would expectedly be small at low Ru concentrations (0.1 – 0.2 wt%) and so would be the positive charge carried by the affected cobalt atoms. At higher Ru loadings, the flow of electrons from Co to Ru would be enhanced thereby increasing the positive charge density on cobalt atoms and, consequently, their oxophilicity. This effect would be more marked for the cobalt atoms on the outermost surface of the nanoparticles, where the concentration of Ru sharply raised for Ru contents above 0.2 wt% (Table 3). The higher oxophilic character of the surface Co atoms in CoRu0.7/Ti and CoRu1.2/Ti would result in a stronger chemisorption of O species originating from CO dissociation leading to the surface Co oxide-like patches (CoO_x) detected in these catalysts. Since the electronic effect is foreseen to be more pronounced at higher Ru contents, the surface Co atoms in CoRu1.2/Ti would be even more positively charged (i.e., more oxophilic) than those in CoRu0.7/Ti. Consequently, more oxygen atoms will irreversibly bind to cobalt upon CO dissociation resulting in "more oxidized" CoO_x patches. This is in agreement with the Wagner plot, where the α' value for the oxide-like species in CoRu1.2/Ti was close to that of the reference Co_3O_4 while it resembled more that of CoO in CoRu0.7/Ti (Figure 7b). The formation of CoO_x patches would lower the amount of metallic Co available for reaction on the surface of Co nanoparticles and would, thus, contribute to the decrease in MTY and (apparent) TOF_0 observed at Ru contents above 0.2 wt% (Table 2). The formation of the detected surface CoO_x patches at high Ru concentrations arising from the electronic interaction between Co and surrounding Ru atoms is schematically depicted in Figure 8.

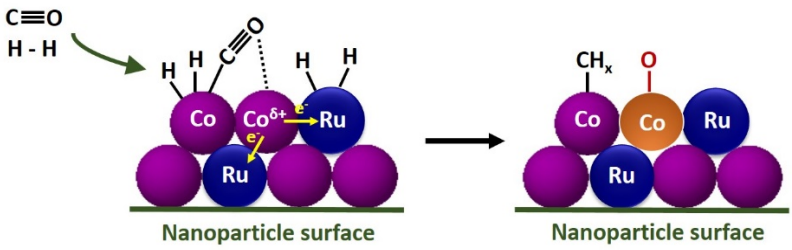

Figure 8. Schematic representation of the formation of surface Co-O species on positively charged surface Co atoms in $CoRu/TiO_2$ catalysts at high promoter concentrations (> 0.2 wt%).

Finally, a shoulder at a higher KE of 779.5 eV in the main Co^0 peak, resulting in α' of 1557.3 eV, is observed for the Co/Ti catalyst (Figure 7a). According to the Wagner plot, this species can neither be attributed to oxidic (CoO_x) nor to metallic (Co^0) cobalt. In a previous study, the shift of the Co LMM Auger peak of metallic Co towards higher KE was associated to the formation of a cobalt carbide phase [52]. Therefore, it seems reasonable to assign the shoulder at KE of 779.5 eV in the Co/Ti catalyst to surface cobalt carbide species. In order to further support this assignment, we measured the Co2p XPS and Co LMM Auger spectra for a Na-promoted Co/SiO_2 sample [61] submitted to in situ reduction with H_2 at 400 °C and subsequent carburization with pure CO at 290 °C and 3.5 bar. The corresponding Co2p XPS and Co LMM Auger spectra after reduction and after carburization, along with the experimental conditions employed for the preparation and in situ activation of the Na-Co/SiO_2 sample, are described in Figure S19 of Supporting Information. As shown there, no cobalt carbide peak could be discerned in the Co2p XPS spectrum of the carburized sample. However, the Co LMM Auger spectrum of the CO-treated sample exhibits, besides a main peak at KE of 773.7 eV of metallic Co (α´ of 1551.6 eV), a shoulder at a higher KE of ca. 779.3 eV (absent in the spectrum of the H_2-reduced sample), corresponding to α´ of 1557.2 eV. Thus, based on this result and on the literature [52], we attribute the shoulder at KE of 779.5 eV (α´ = 1557.3 eV) observed in the Co LMM Auger spectrum of the Ru-free Co/Ti catalyst (Figure 7a, spectrum d) to the formation of a surface cobalt carbide phase during FTS reaction. This seems in line with the results of the FTIR-syngas study at 1 bar, where a lower ability of the unpromoted catalyst for desorbing surface carbon intermediates during FTS compared to the Ru-promoted samples was inferred (Figure 6). The formation of surface carbide-like cobalt patches in the Ru-free catalyst also aligns with preceding studies, where the reduced hydrogenation ability in the absence of Ru was shown to boost the deposition of carbonaceous species on the surface of Co/TiO_2 catalysts, reducing the concentration of accessible Co^0 sites and, consequently, the FTS activity since the early reaction stages [9].

The formation, during reaction, of FTS-inactive surface carbide-like and oxide-like cobalt patches in the absence of Ru promoter and at high Ru contents (0.7 – 1.2 wt%), respectively, is visually shown in Figure 9.

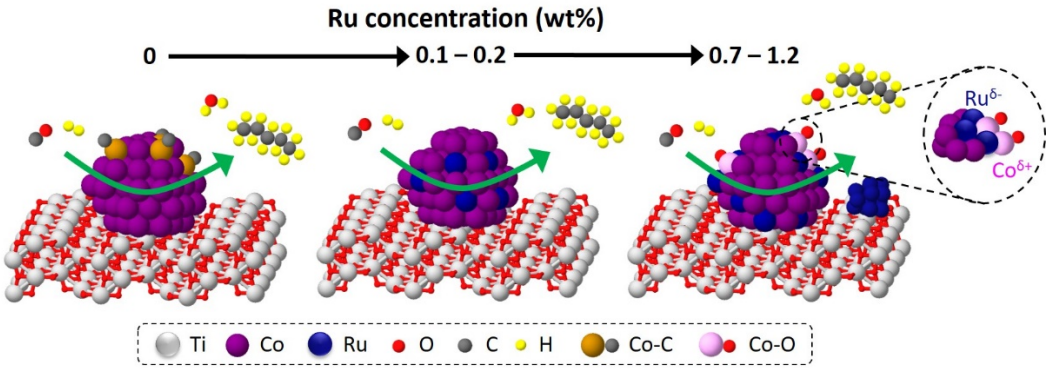

Figure 9. Schematic representation of the influence of Ru addition and Ru content on the nature of surface cobalt species under FTS conditions, according to Co LMM Auger characterization, showing the formation of Co-C in the absence of Ru and of Co-O at high Ru contents (> 0.2 wt%).

Based on the previous characterizations and the XPS-Auger spectroscopic results discussed above, the volcano-type dependence of the FTS activity with the Ru content can be accounted for by considering the following factors: 1) the formation of surface CoC_x patches and a more extended SMSI effect in the absence of promoter, and 2) the presence of surface CoO_x species and a higher proportion of intrinsically less active sub-6 nm nanoparticles at Ru concentrations above 0.2 wt%.

4. Conclusions

In conclusion, the in situ characterization by means of XAS, FTIR, and XPS-Auger spectroscopies reported in the present work provided useful insights into the genesis of the effects of promotion with Ru of Co/TiO_2 catalysts for the FTS reaction that were otherwise unfeasible by using conventional ex situ methods. At industrially relevant FTS conditions (220 °C, 20 bar, H_2/CO= 2), the Ru-promoted catalysts presented both higher activity per total mass of metal (MTY, metal-time yield) and C_{5+} selectivity than an equivalent Ru-free catalyst. As with MTY, initial *turnover* rates (TOF_0) exhibited a volcano-type dependence with Ru content, achieving maximum values for the catalysts promoted with low amounts of Ru (0.1 – 0.2 wt%). Our results suggested that morphological changes and electronic interactions between adjacent Co and Ru atoms on the surface of bimetallic Co-Ru nanoparticles are behind the observed promotion effects. Thus, FTIR experiments under flowing syngas at 220 °C and 1 bar indicated the occurrence of surface reconstruction of the Co nanoparticles creating more defected Co^0 sites with enhanced intrinsic FTS reactivity (TOF) only in the Ru-promoted catalysts, and signed for a stronger SMSI decoration effect in the unpromoted Co/TiO_2 catalyst under reaction conditions. Interestingly, the analysis of the Co

LMM Auger peaks through the modified Auger parameter (α') and the Wagner plot revealed that, while the surface of Co nanoparticles in the most active catalysts (0.1 – 0.2 wt% Ru) remained metallic during FTS (220 °C and 9 bar), it was partly covered by oxide-like cobalt (e.g., CoO_x) patches at high Ru loading (> 0.2 wt%). We propose that this could arise from a partial electron charge transfer from Co^0 to the more electronegative adjacent Ru^0 atoms promoting the irreversible adsorption of surface O adatoms formed upon CO dissociation on positively charged Co atoms (e.g., $Co^{\delta+}$) at high Ru concentrations. On the other hand, the presence of carbide-like cobalt patches (e.g., CoC_x) was identified on the surface of the Co nanoparticles in the monometallic Co/TiO_2 catalyst as the result of a reduced hydrogenation capacity in the absence of Ru. In spite of the metallic character of the bulk Co nanoparticles, the presence of such oxide- and carbide-like Co patches in these catalysts could thus contribute to their lower apparent TOF_0 compared to the most active catalyst promoted with 0.2 wt% Ru. Moreover, the increased proportion of intrinsically less active sub-6 nm Co^0 nanoparticles may also add to the decrease in TOF_0 (and MTY) observed for the Ru-promoted catalysts at promoter contents beyond 0.2 wt%.

Supporting Information

Methods for conventional characterizations, FTS activity of Ru/TiO_2, characterization of TiO_2-anatase support (XRD, FESEM, N_2 physisorption), characterization of calcined catalysts (XRD, N_2 physisorption, H_2-TPR), EDS mapping, CO-FTIR, XAS, XPS, and in situ XRD characterization of H_2-reduced catalysts, ASF distribution and olefin/paraffin ratio of hydrocarbons, in situ EXAFS, CO-FTIR and XPS characterization under FTS conditions.

Acknowledgments

Financial support by the MINECO of Spain through the Severo Ochoa (SEV2016-0683) and RTI2018-102161 projects is gratefully acknowledged. The authors are thankful to the Microscopy Service of the Universitat Politècnica de València for its assistance in microscopy characterization. XAS experiments at ambient pressure were performed on beamline BM23 at the European Synchrotron Radiation Facility (ESRF), Grenoble, France. We are grateful to Debora Motta Meira at the ESRF for providing assistance in using beamline BM23. Thanks are also due to ALBA synchrotron for allocating beamtime (XAS experiments at higher pressure) and CLÆSS beamline staff for their technical support during the experiment. F.B. (Science without Borders − Process no. 13705/13-0) and C.W.L. (Science without Borders − Process no. 13191/13-6) thank CAPES for a predoctoral fellowship. A.C.F.

and E.A.S. acknowledge support to Integrated Mesoscale Architectures for Sustainable Catalysis (IMASC), an Energy Frontier Research Center funded by the U.S. Department of Energy, Office of Science, Basic Energy Sciences under Award # DE-SC0012573.

References

1. Khodakov, A. Y.; Chu, W.; Fongarland, P., Advances in the development of novel cobalt Fischer-Tropsch catalysts for synthesis of long-chain hydrocarbons and clean fuels. *Chem. Rev.* **2007,** *107* (5), 1692-744.

2. Beaumont, S. K., Recent developments in the application of nanomaterials to understanding molecular level processes in cobalt catalysed Fischer-Tropsch synthesis. *Phys. Chem. Chem. Phys.* **2014,** *16* (11), 5034-5043.

3. Li, J.; Jacobs, G.; Zhang, Y.; Das, T.; Davis, B. H., Fischer–Tropsch synthesis: effect of small amounts of boron, ruthenium and rhenium on Co/TiO2 catalysts. *Applied Catalysis A: General* **2002,** *223* (1), 195-203.

4. Shannon, M. D.; Lok, C. M.; Casci, J. L., Imaging promoter atoms in Fischer–Tropsch cobalt catalysts by aberration-corrected scanning transmission electron microscopy. *Journal of Catalysis* **2007,** *249* (1), 41-51.

5. Girardon, J.; Quinet, E.; Gribovalconstant, A.; Chernavskii, P.; Gengembre, L.; Khodakov, A., Cobalt dispersion, reducibility, and surface sites in promoted silica-supported Fischer–Tropsch catalysts. *Journal of Catalysis* **2007,** *248* (2), 143-157.

6. Tsubaki, N.; Sun, S.; Fujimoto, K., Different Functions of the Noble Metals Added to Cobalt Catalysts for Fischer–Tropsch Synthesis. *Journal of Catalysis* **2001,** *199* (2), 236-246.

7. Kogelbauer, A.; Goodwin, J. J. G.; Oukaci, R., Ruthenium Promotion of Co/Al2O3Fischer–Tropsch Catalysts. *Journal of Catalysis* **1996,** *160* (1), 125-133.

8. Trépanier, M.; Tavasoli, A.; Dalai, A. K.; Abatzoglou, N., Co, Ru and K loadings effects on the activity and selectivity of carbon nanotubes supported cobalt catalyst in Fischer–Tropsch synthesis. *Applied Catalysis A: General* **2009,** *353* (2), 193-202.

9. Iglesia, E.; Soled, S. L.; Fiato, R. A.; Via, G. H., Bimetallic Synergy in Cobalt Ruthenium Fischer-Tropsch Synthesis Catalysts. *Journal of Catalysis* **1993,** *143* (2), 345-368.

10. Zhang, H.; Chu, W.; Zou, C.; Huang, Z.; Ye, Z.; Zhu, L., Promotion Effects of Platinum and Ruthenium on Carbon Nanotube Supported Cobalt Catalysts for Fischer-Tropsch Synthesis. *Catal. Lett.* **2011,** *141* (3), 438-444.

11. Xiong, H.; Zhang, Y.; Liew, K.; Li, J., Ruthenium promotion of Co/SBA-15 catalysts with high cobalt loading for Fischer-Tropsch synthesis. *Fuel Process. Technol.* **2009,** *90* (2), 237-246.

12. Jacobs, G.; Das, T. K.; Zhang, Y.; Li, J.; Racoillet, G.; Davis, B. H., Fischer–Tropsch synthesis: support, loading, and promoter effects on the reducibility of cobalt catalysts. *Applied Catalysis A: General* **2002,** *233* (1-2), 263-281.

13. Ma, W.; Jacobs, G.; Keogh, R. A.; Bukur, D. B.; Davis, B. H., Fischer–Tropsch synthesis: Effect of Pd, Pt, Re, and Ru noble metal promoters on the activity and selectivity of a 25%Co/Al2O3 catalyst. *Applied Catalysis A: General* **2012,** *437-438*, 1-9.

14. Han, Q.; Yao, N.; Shi, Y.; Ma, H.; Li, X., Improvement the promotional efficiency of Ru by controlling the position and distribution of RuO2 precursors on CoRu/SiO2 catalyst. *Catalysis Communications* **2012,** *22*, 52-57.

15. Eschemann, T. O.; Oenema, J.; de Jong, K. P., Effects of noble metal promotion for Co/TiO 2 Fischer-Tropsch catalysts. *Catalysis Today* **2016,** *261*, 60-66.

16. Hong, J.; Marceau, E.; Khodakov, A. Y.; Gaberová, L.; Griboval-Constant, A.; Girardon, J.-S.; Fontaine, C. L.; Briois, V., Speciation of Ruthenium as a Reduction Promoter of Silica-Supported Co Catalysts: A Time-Resolved in Situ XAS Investigation. *ACS Catalysis* **2015,** *5* (2), 1273-1282.

17. Coronel-Garcia, M. A.; Reyes de la Torre, A. I.; Melo-Banda, J. A.; Martinez-Salazar, A. L.; Silva Rodrigo, R.; Diaz Zavala, N. P.; Portales Martinez, B.; Dominguez, J. M., Study of Co, Ru/SBA-15 type materials for Fischer-Tropsch synthesis in fixed bed tubular reactor: I. Effect of the high Ru content on the catalytic activity. *Int. J. Hydrogen Energy* **2015,** *40* (48), 17264-17271.

18. Parnian, M. J.; Taheri Najafabadi, A.; Mortazavi, Y.; Khodadadi, A. A.; Nazzari, I., Ru promoted cobalt catalyst on γ-Al2O3: Influence of different catalyst preparation method and Ru loadings on Fischer-Tropsch reaction and kinetics. *Appl. Surf. Sci.* **2014,** *313*, 183-195.

19. Park, J.-Y.; Lee, Y.-J.; Karandikar, P. R.; Jun, K.-W.; Bae, J. W.; Ha, K.-S., Ru promoted cobalt catalyst on γ-Al2O3 support: Influence of pre-synthesized nanoparticles on Fischer–Tropsch reaction. *Journal of Molecular Catalysis A: Chemical* **2011,** *344* (1-2), 153-160.

20. Hosseini, S. A.; Taeb, A.; Feyzi, F.; Yaripour, F., Fischer–Tropsch synthesis over Ru promoted Co/γ-Al2O3 catalysts in a CSTR. *Catalysis Communications* **2004,** *5* (3), 137-143.

21. Agostini, G.; Meira, D.; Monte, M.; Vitoux, H.; Iglesias-Juez, A.; Fernandez-Garcia, M.; Mathon, O.; Meunier, F.; Berruyer, G.; Perrin, F.; Pasternak, S.; Mairs, T.; Pascarelli, S.; Gorges, B., XAS/DRIFTS/MS spectroscopy for time-resolved operando investigations at high temperature. *J. Synchrotron Radiat.* **2018,** *25* (6), 1745-1752.

22. Ravel, B.; Newville, M., ATHENA, ARTEMIS, HEPHAESTUS: data analysis for X-ray absorption spectroscopy using IFEFFIT. *Journal of Synchrotron Radiation* **2005,** *12* (4), 537-541.

23. Prieto, G.; Martínez, A.; Concepción, P.; Moreno-Tost, R., Cobalt particle size effects in Fischer–Tropsch synthesis: structural and in situ spectroscopic characterisation on reverse micelle-synthesised Co/ITQ-2 model catalysts. *Journal of Catalysis* **2009,** *266* (1), 129-144.

24. Storsater, S.; Totdal, B.; Walmsley, J.; Tanem, B.; Holmen, A., Characterization of alumina-, silica-, and titania-supported cobalt Fischer–Tropsch catalysts. *Journal of Catalysis* **2005,** *236* (1), 139-152.

25. Agostini, G.; Piovano, A.; Bertinetti, L.; Pellegrini, R.; Leofanti, G.; Groppo, E.; Lamberti, C., Effect of Different Face Centered Cubic Nanoparticle Distributions on Particle Size and Surface Area Determination: A Theoretical Study. *The Journal of Physical Chemistry C* **2014,** *118* (8), 4085-4094.

26. Morgan, D. J., Resolving ruthenium: XPS studies of common ruthenium materials. *Surf. Interface Anal.* **2015,** *47* (11), 1072-1079.

27. Niu, X.; Tang, Q.; He, B.; Yang, P., Robust and stable ruthenium alloy electrocatalysts for hydrogen evolution by seawater splitting. *Electrochim. Acta* **2016,** *208*, 180-187.

28. Karaca, H.; Safonova, O. V.; Chambrey, S.; Fongarland, P.; Roussel, P.; Griboval-Constant, A.; Lacroix, M.; Khodakov, A. Y., Structure and catalytic performance of Pt-promoted alumina-supported cobalt catalysts under realistic conditions of Fischer–Tropsch synthesis. *Journal of Catalysis* **2011,** *277* (1), 14-26.

29. Lyu, S.; Wang, L.; Zhang, J.; Liu, C.; Sun, J.; Peng, B.; Wang, Y.; Rappé, K. G.; Zhang, Y.; Li, J.; Nie, L., Role of Active Phase in Fischer–Tropsch Synthesis: Experimental Evidence of CO Activation over Single-Phase Cobalt Catalysts. *ACS Catalysis* **2018,** *8* (9), 7787-7798.

30. Bezemer, G. L.; Bitter, J. H.; Kuipers, H. P.; Oosterbeek, H.; Holewijn, J. E.; Xu, X.; Kapteijn, F.; van Dillen, A. J.; de Jong, K. P., Cobalt particle size effects in the Fischer-Tropsch reaction studied with carbon nanofiber supported catalysts. *J Am Chem Soc* **2006,** *128* (12), 3956-64.

31. Martínez, A.; Prieto, G.; Rollán, J., Nanofibrous γ-Al2O3 as support for Co-based Fischer–Tropsch catalysts: Pondering the relevance of diffusional and dispersion effects on catalytic performance. *Journal of Catalysis* **2009,** *263* (2), 292-305.

32. Bertella, F.; Concepción, P.; Martínez, A., TiO2 polymorph dependent SMSI effect in Co-Ru/TiO2 catalysts and its relevance to Fischer-Tropsch synthesis. *Catalysis Today* **2017,** *289*, 181-191.

33. Bertella, F.; Concepción, P.; Martínez, A., The impact of support surface area on the SMSI decoration effect and catalytic performance for Fischer-Tropsch synthesis of Co-Ru/TiO 2 -anatase catalysts. *Catalysis Today* **2017,** *296*, 170-180.

34. Weststrate, C. J.; van Helden, P.; Niemantsverdriet, J. W., Reflections on the Fischer-Tropsch synthesis: Mechanistic issues from a surface science perspective. *Catalysis Today* **2016,** *275*, 100-110.

35. Banerjee, A.; van Bavel, A. P.; Kuipers, H. P. C. E.; Saeys, M., CO Activation on Realistic Cobalt Surfaces: Kinetic Role of Hydrogen. *ACS Catalysis* **2017,** *7* (8), 5289-5293.

36. Iglesia, E., Design, synthesis, and use of cobalt-based Fischer-Tropsch synthesis catalysts. *Applied Catalysis A: General* **1997,** *161* (1-2), 59-78.

37. Prieto, G.; De Mello, M. I. S.; Concepción, P.; Murciano, R.; Pergher, S. B. C.; Martínez, A. n., Cobalt-Catalyzed Fischer–Tropsch Synthesis: Chemical Nature of the Oxide Support as a Performance Descriptor. *ACS Catalysis* **2015,** *5* (6), 3323-3335.

38. Fredriksen, G. R.; Blekkan, E. A.; Schanke, D.; Holmen, A., CO hydrogenation over supported cobalt catalysts: FTIR and gravimetric studies. *Chemical Engineering & Technology* **1995,** *18* (2), 125-131.

39. Rygh, L. E. S.; Ellestad, O. H.; Klæboe, P.; Nielsen, C. J., Infrared study of CO adsorbed on Co/γ-Al2O3 based Fischer–Tropsch catalysts; semi-empirical calculations as a tool for vibrational assignments. *Physical Chemistry Chemical Physics* **2000,** *2* (8), 1835-1846.

40. Jiang, M.; Koizumi, N.; Ozaki, T.; Yamada, M., Adsorption properties of cobalt and cobalt-manganese catalysts studied by in situ diffuse reflectance FTIR using CO and CO+H2 as probes. *Applied Catalysis A: General* **2001,** *209* (1-2), 59-70.

41. Rao, K. M.; Spoto, G.; Zecchina, A., IR investigation of CO adsorbed on Co particles obtained via Co2(CO)8 adsorbed on MgO and SiO2. *Journal of Catalysis* **1988,** *113* (2), 466-474.

42. Busca, G.; Guidetti, R.; Lorenzelli, V., Fourier-transform infrared study of the surface properties of cobalt oxides. *Journal of the Chemical Society, Faraday Transactions* **1990,** *86* (6), 989.

43. Kadinov, G.; Bonev, C.; Todorova, S.; Palazov, A., IR spectroscopy study of CO adsorption and of the interaction between CO and hydrogen on alumina-supported cobalt. *Journal of the Chemical Society, Faraday Transactions* **1998,** *94* (19), 3027-3031.

44. Iglesia, E.; Soled, S. L.; Fiato, R. A., Fischer-Tropsch synthesis on cobalt and ruthenium. Metal dispersion and support effects on reaction rate and selectivity. *Journal of Catalysis* **1992,** *137* (1), 212-224.

45. Visconti, C. G.; Lietti, L.; Tronconi, E.; Forzatti, P.; Zennaro, R.; Finocchio, E., Fischer–Tropsch synthesis on a Co/Al2O3 catalyst with CO2 containing syngas. *Applied Catalysis A: General* **2009,** *355* (1-2), 61-68.

46. Smith, B. C., How to Properly Compare Spectra, and Determining Alkane Chain Length From Infrared Spectra. *Spectroscopy* **2015,** *30* (9), 40-46.

47. Rygh, L. E. S.; Nielsen, C. J., Infrared Study of CO Adsorbed on a Co/Re/γAl2O3-Based Fischer–Tropsch Catalyst. *Journal of Catalysis* **2000,** *194* (2), 401-409.

48. Petersen, M. A.; van den Berg, J.-A.; Ciobica, I. M.; van Helden, P., Revisiting CO Activation on Co Catalysts: Impact of Step and Kink Sites from DFT. *ACS Catal.* **2017,** *7* (3), 1984-1992.

49. Ciobica, I. M.; van Santen, R. A.; van Berge, P. J.; van de Loosdrecht, J., Adsorbate induced reconstruction of cobalt surfaces. *Surf. Sci.* **2008,** *602* (1), 17-27.

50. Zhang, F.-Y.; Advani, S. G.; Prasad, A. K.; Boggs, M. E.; Sullivan, S. P.; Beebe, T. P., Quantitative characterization of catalyst layer degradation in PEM fuel cells by X-ray photoelectron spectroscopy. *Electrochimica Acta* **2009,** *54* (16), 4025-4030.

51. Li, M.; Boggs, M.; Beebe, T. P.; Huang, C. P., Oxidation of single-walled carbon nanotubes in dilute aqueous solutions by ozone as affected by ultrasound. *Carbon* **2008,** *46* (3), 466-475.

52. Ye, D. X.; Pimanpang, S.; Jezewski, C.; Tang, F.; Senkevich, J. J.; Wang, G. C.; Lu, T. M., Low temperature chemical vapor deposition of Co thin films from Co2(CO)8. *Thin Solid Films* **2005,** *485* (1-2), 95-100.

53. Biesinger, M. C.; Payne, B. P.; Grosvenor, A. P.; Lau, L. W. M.; Gerson, A. R.; Smart, R. S. C., Resolving surface chemical states in XPS analysis of first row transition metals, oxides and hydroxides: Cr, Mn, Fe, Co and Ni. *Applied Surface Science* **2011,** *257* (7), 2717-2730.

54. Powell, C. J., Recommended Auger parameters for 42 elemental solids. *Journal of Electron Spectroscopy and Related Phenomena* **2012,** *185* (1-2), 1-3.

55. NIST: National Institute of Standards and Technology.

56. Ananthan, S. A.; Suresh, R.; Giribabu, K.; Narayanan, V., Synthesis and characterization of bimetallic nanocatalysts and their application in selective hydrogenation of citral to unsaturated alcohols. *Journal of Chemical Sciences* **2013,** *125* (6), 1365-1374.

57. Logsdail, A. J.; Paz-Borbon, L. O.; Downing, C. A., DFT-Computed Trends in the Properties of Bimetallic Precious Metal Nanoparticles with Core@Shell Segregation. *J. Phys. Chem. C* **2018,** *122* (10), 5721-5730.

58. Chen, T.; Rodionov, V. O., Controllable Catalysis with Nanoparticles: Bimetallic Alloy Systems and Surface Adsorbates. *ACS Catalysis* **2016,** *6* (6), 4025-4033.

59. Singh, A. K.; Xu, Q., Synergistic Catalysis over Bimetallic Alloy Nanoparticles. *ChemCatChem* **2013,** *5* (3), 652-676.

60. Sankar, M.; Dimitratos, N.; Miedziak, P. J.; Wells, P. P.; Kiely, C. J.; Hutchings, G. J., Designing bimetallic catalysts for a green and sustainable future. *Chemical Society Reviews* **2012,** *41* (24), 8099-8139.

61. Gnanamani, M. K.; Jacobs, G.; Keogh, R. A.; Shafer, W. D.; Sparks, D. E.; Hopps, S. D.; Thomas, G. A.; Davis, B. H., Fischer-Tropsch synthesis: Effect of pretreatment conditions of cobalt on activity and selectivity for hydrogenation of carbon dioxide. *Applied Catalysis A: General* **2015,** *499*, 39-46.

For Table of Contents Only

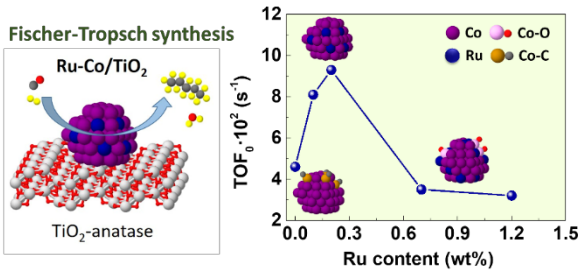

Supporting Information

for

Insights into the promotion with Ru of Co/TiO_2 Fischer-Tropsch catalysts: An in situ spectroscopic study

Francine Bertella[a,b], Christian W. Lopes[a,b], Alexandre C. Foucher[d], Giovanni Agostini[c], Patricia Concepción[a], Eric A. Stach[d], Agustín Martínez[a,*]

[a] *Instituto de Tecnología Química, Universitat Politècnica de València - Consejo Superior de Investigaciones Científicas (UPV-CSIC), Avda. de los Naranjos s/n, 46022 Valencia, Spain.*

[b] *Institute of Chemistry, Universidade Federal do Rio Grande do Sul – UFRGS, Av. Bento Gonçalves, 9500, P.O. Box 15003, 91501-970 Porto Alegre, RS, Brazil.*

[c] *CELLS – ALBA Synchrotron Radiation Facility, Carrer de la Llum 2-26, 08290 Cerdanyola del Vallès, Barcelona, Spain.*

[d] *Department of Materials Science and Engineering, University of Pennsylvania, Philadelphia, Pennsylvania 19104, United States.*

* Corresponding author: amart@itq.upv.es (A. Martínez)

1. Characterization of catalysts by conventional techniques

Cobalt and ruthenium contents were determined by Inductively Coupled Plasma-Optical Emission Spectrometry (ICP-OES) in a Varian 715-ES spectrometer after dissolving the samples in an acid mixture of HNO_3:HF:HCl (1:1:3 volume ratio).

X-ray powder diffraction (XRD) was performed on the calcined materials with a Philips X'Pert diffractometer using monochromatized Cu K_α radiation (λ = 0.15406 nm). Average TiO_2 particle sizes were calculated from the most intense (101) reflection of anatase (2θ = 25.3°) using the Scherrer's equation and assuming a shape factor k = 0.9.

In situ H_2-XRD measurements were performed to assess the crystalline phases present in the as-reduced catalysts. The measurements were performed in a Panalytical Empyrean diffractometer using Cu K_α radiation. The samples were loaded in an XRK 900 Anton Paar reaction chamber and flushed with a gas stream comprising 10 vol% H_2 diluted in N_2. In these experiments, the X-ray diffractograms were first recorded at 25 °C (corresponding to the calcined state of the catalysts) and then the temperature was raised to 400 °C under the diluted H_2 flow with a ramping of 2 °C/min. XRD patterns were recorded at selected times after reaching the final reduction temperature.

Nitrogen adsorption isotherms were measured in a Micromeritics ASAP-2420 equipment at liquid N_2 temperature (-196 °C). Prior to the analyses, the samples were degassed at 300 °C under vacuum overnight. Specific surface areas were determined following the Brunauer-Emmett-Teller (BET) method, pore size distributions were derived by applying the Barrett-Joyner-Halenda (BJH) approach to the adsorption branch of the isotherms, and total pore volumes were obtained at a relative pressure of 0.98.

Morphological analysis of the support was performed by field emission scanning electron microscopy (FESEM) using a ZEISS Ultra-55 microscope after depositing the sample powder on a double-sided tape.

H_2 temperature-programmed reduction (H_2-TPR) was carried out using a Micromeritics Autochem 2910 device. Typically, 55 mg of catalyst were initially flushed with an Ar flow at room temperature for 30 min. Subsequently, the gas atmosphere was switched to 10 vol% H_2 diluted in Ar. Next, the temperature was linearly increased up to 900 °C at a heating rate of 10 °C/min and the H_2 consumption monitored in a thermal conductivity detector (TCD) previously calibrated using the reduction of a standard CuO sample. A 2-propanol/$N_{2(liq)}$ trap located downstream the analyzer was used to retain the water generated in the reduction. The degree of cobalt reduction (DOR) was

determined in the same equipment on catalysts previously reduced in situ at the same conditions applied prior the FTS reaction (i.e., at 400 °C for 10 h under flowing pure H_2). Then, after switching to the diluted H_2 stream (10 vol% H_2 in Ar), the temperature was increased from 400 °C to 900 °C with a ramping of 10 °C/min and the H_2 consumption monitored in the TCD. The DOR was calculated from the amount of H_2 consumed, assuming that this corresponds to the reduction of CoO remaining in the catalyst after the initial reduction treatment in pure H_2 at 400 °C.

The concentration of surface metal sites was measured by H_2 chemisorption at 100 °C for Co/Ti and CoRu*x*/Ti [1] and at 75 °C for Ru/Ti [2] in a Quantachrome Autosorb-1C instrument by extrapolating the total gas uptakes in the adsorption isotherms at zero pressure. Before measurements, the oxide catalyst precursors were reduced under pure H_2 flow at 400 °C for 10 h.

Direct measurement of cobalt particle sizes was performed by transmission electron microscopy in a JEOL-JEM 2100F microscope operating at 200 kV in scanning transmission mode (STEM) using a high-angle annular dark field (HAADF) detector. Energy dispersive X-ray spectroscopy (EDS) was used to study the spatial distribution of Co and Ru species in the samples using an X-Max 80 detector from Oxford Instruments equipped with Aztec software. Before microscopy observation, the samples were reduced ex situ in flowing pure H_2 at 400 °C for 10 h, passivated at room temperature under a flow of 0.5 vol% O_2/N_2, suspended in isopropanol, and ultrasonicated for one minute. The suspension was let to decant and a drop was extracted from the top side and deposited on a carbon-coated copper grid. STEM-derived cobalt particle sizes and particle size distributions were obtained after measuring 200-300 particles from several micrographs taken at different positions on the TEM grid and correcting for the presence of a 2.5 nm thick CoO passivation outlayer [3]. Surface average D[3,2] cobalt particle sizes were calculated from the measured particle sizes as: $d(Co^0)_{STEM} = \Sigma n_i \cdot d_i^3 / \Sigma n_i \cdot d_i^2$.

2. Assessment of the FTS activity of segregated Ru species at high promoter concentrations

In order to ascertain whether the monometallic Ru species on the TiO_2 carrier contribute significantly to the overall FTS activity of CoRu*x*/Ti catalysts (*x* = 0.7, 1.2), a Ru/Ti catalyst containing 0.4 wt% Ru after calcination (as measured by ICP-OES) was evaluated at 220 °C, 20 bar, and GHSV = 11.7 $L_{syngas}/(g_{cat}\cdot h)$ for 8 h. At these conditions, the Ru/Ti catalyst displayed a CO conversion of only 0.1%, translating into a Ru-time yield of $4.35\cdot10^{-2}$ $mol_{CO}/(g_{Ru}\cdot h)$. From this value, considering the amount of Ru atoms involved in Ru-Ru species derived from XPS analyses (Figure 3, main text) and assuming that all Ru atoms are available for reaction (ideal case), the relative contribution of monometallic Ru species to the initial MTY of the CoRu0.7/Ti and CoRu1.2/Ti catalysts is estimated to be 2.4 and 5.9%, respectively.

Figure S1. X-ray diffraction pattern of the calcined TiO_2-anatase support.

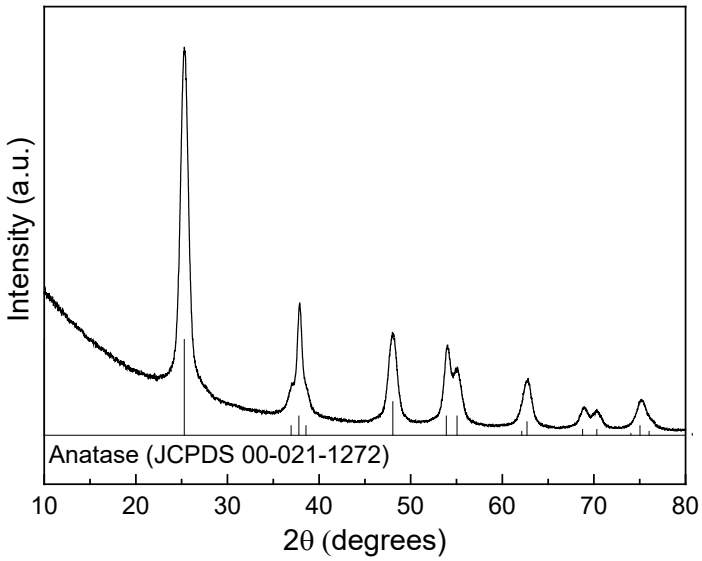

The XRD pattern of the calcined TiO_2 support confirms that the synthesized TiO_2 material consists of pure anatase (JCPDS 00-021-1272) with an average crystallite size of ca. 10 nm, as estimated by line broadening analysis of the most intense diffraction peak at 2θ= 25.3°.

Figure S2. Representative FESEM image for the calcined TiO_2-anatase support.

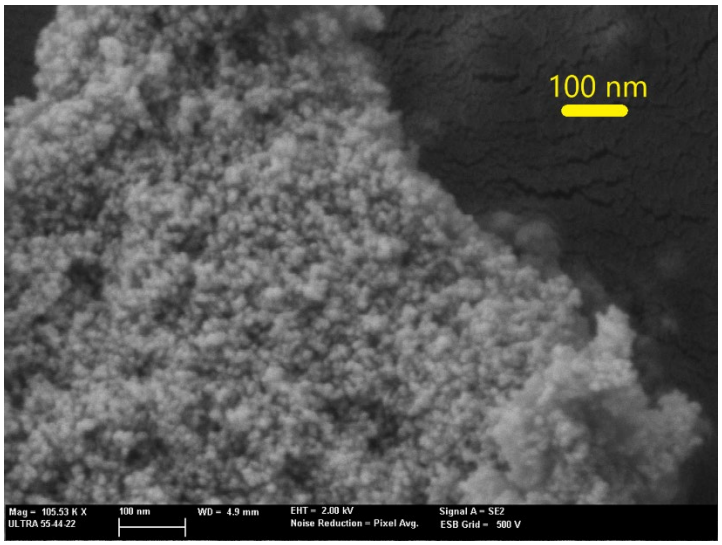

As evidenced in the FESEM image, the material comprises small rice-like crystallites with sizes ranging from 10 to 30 nm, in fair agreement with XRD (Figure S1).

Figure S3. N_2 adsorption-desorption isotherm (a) and BJH pore size distribution (b) for the calcined TiO_2-anatase support.

a) b)

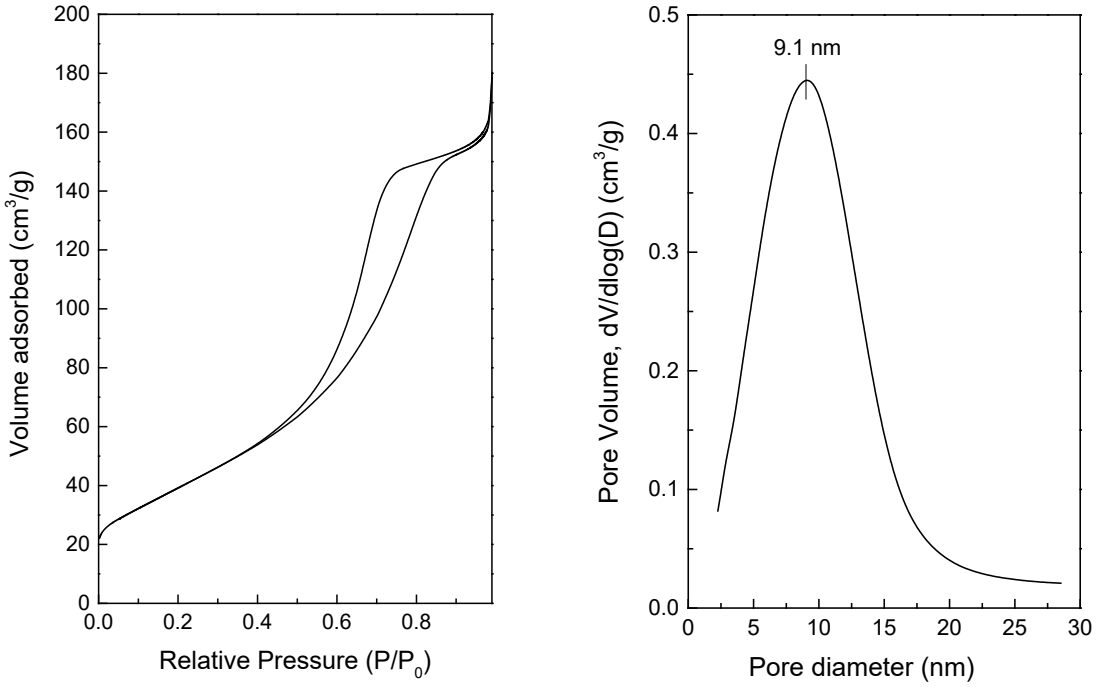

The calcined TiO_2-anatase presents a type IV adsorption-desorption isotherm (panel a), characteristic of mesoporous solids, with a large hysteresis loop at high relative pressures due to capillary condensation, and a unimodal pore size distribution in the mesopore range with maximum at 9.1 nm (panel b).

Figure S4. X-ray diffraction (XRD) patterns of calcined Co/TiO_2 and $CoRu/TiO_2$ catalysts. The characteristic diffraction peaks of Co_3O_4 are marked (*) for an easier identification. The inset shows the reflections related to RuO_2 in the CoRu1.2/Ti catalyst.

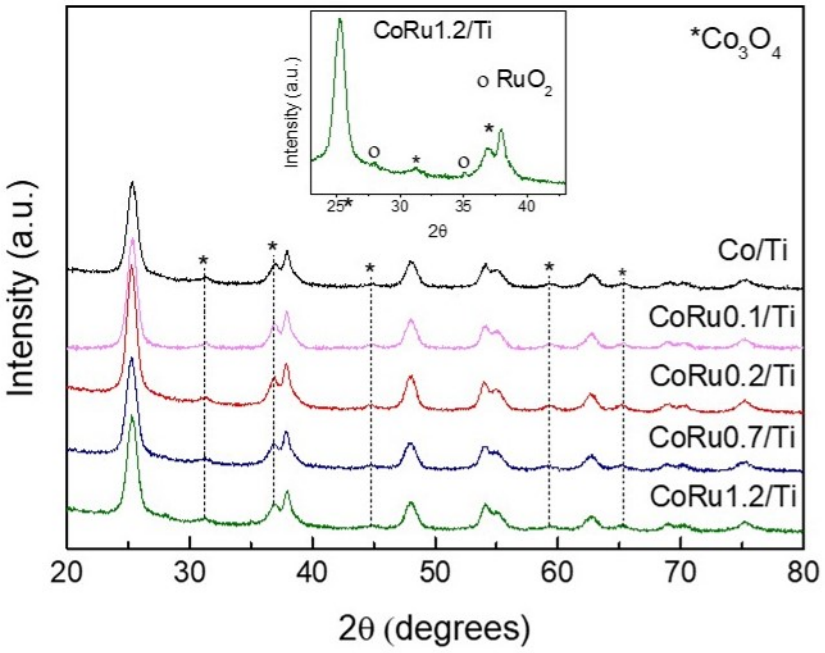

The XRD patterns of the calcined CoRu*x*/Ti and Co/Ti catalysts show, in all cases, the presence of Co_3O_4 (JCPDS 00-042-1467) as the only cobalt crystalline phase. However, a safe assessment of the Co_3O_4 crystallite size by XRD is hampered by the low relative intensity of the Co_3O_4 diffractions and overlapping with anatase-related peaks. Besides, very low intense peaks ascribed to RuO_2 crystallites (JCPDS 00-040-1290) are observed for the CoRu1.2/Ti catalyst with the highest Ru loading (see inset). Moreover, neither the TiO_2 crystalline phase (anatase) nor its mean crystallite size experienced noticeable changes upon impregnation of the support with the metal precursors and subsequent calcination.

Figure S5. N_2 adsorption isotherms (a) and corresponding pore size distributions (b) for calcined Co/TiO_2 and $CoRu/TiO_2$ catalysts. For the sake of clarity, the isotherms in panel a) for catalysts CoRu0.1/Ti, CoRu0.2/Ti, CoRu0.7/Ti, and CoRu1.2/Ti have been upshifted by 10, 20, 30, and 40 cm^3/g, respectively.

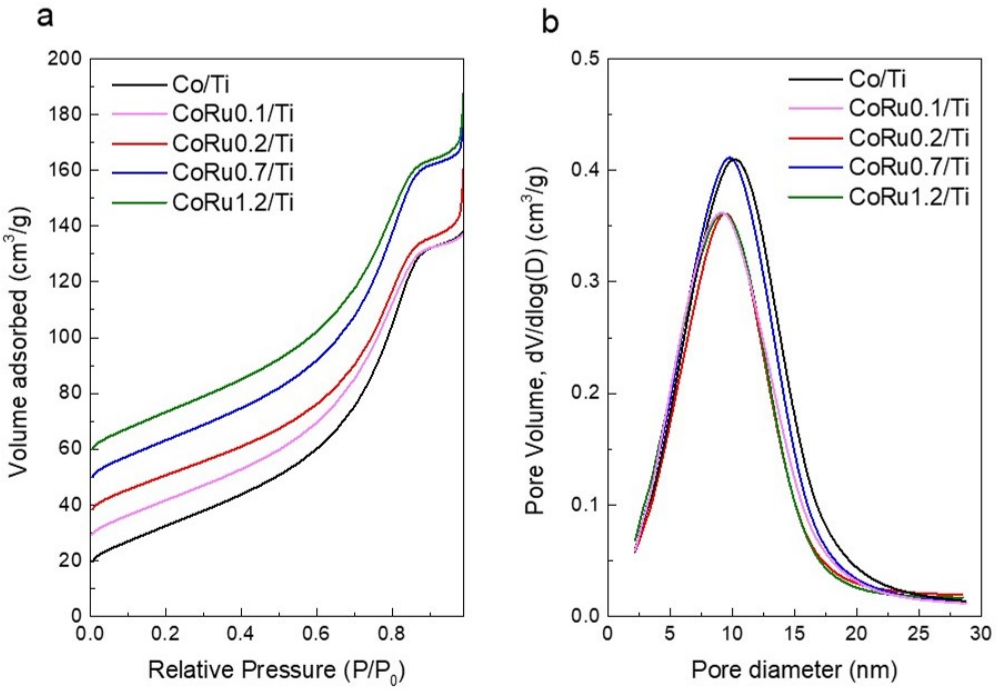

The calcined catalysts exhibit, similar to the bare TiO_2 support, type IV N_2 adsorption isotherms (panel a), reflecting their mesoporous character, and unimodal pore size distributions with maxima at ca. 9-10 nm (panel b).

Table S1. Textural properties derived from N_2 adsorption isotherms for Co/TiO_2 and $CoRu/TiO_2$ catalysts.

Catalyst	BET area[a] (m^2/g)	Pore diameter (nm)	Total pore volume[a] (cm^3/g)
TiO_2	148	9.1	0.25
Co/Ti	112 (134)	9.9	0.21 (0.25)
CoRu0.1/Ti	116 (139)	9.2	0.20 (0.24)
CoRu0.2/Ti	113 (135)	9.7	0.20 (0.24)
CoRu0.7/Ti	112 (134)	9.8	0.22 (0.26)
CoRu1.2/Ti	116 (141)	9.7	0.21 (0.25)

[a] Values in parentheses correspond to the values normalized per mass of TiO_2 support.

A decrease in the BET surface area of 22-24% with respect to the pristine support is noticed for all catalysts. However, when normalized per mass of support (values in parenthesis), the relative decrease in BET area is lower than 10% in all cases which, besides the alike values of mean pore diameter and pore volume for catalysts and support, indicate negligible pore blockage in the catalysts by the supported metal oxides.

Figure S6. H_2-TPR profiles for unpromoted (Co/Ti) and Ru-promoted (CoRu*x*/Ti) catalysts (*x* = 0.1, 0.2, 0.7, 1.2 wt% Ru).

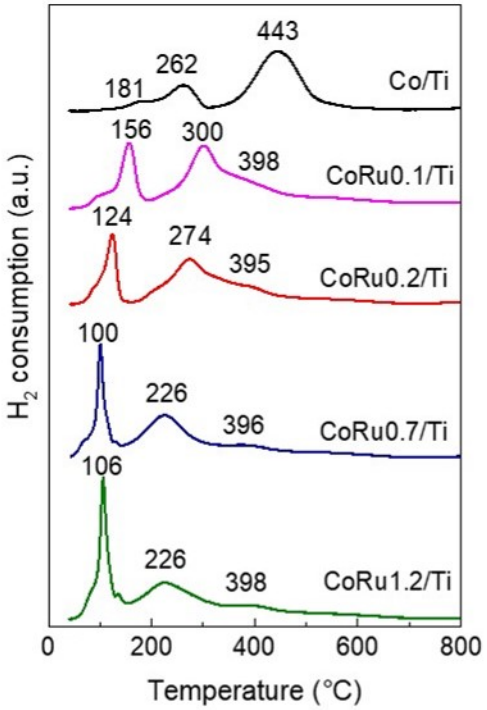

As commonly found for *ex*-nitrate supported Co catalysts [4,5], the reduction of Co_3O_4 takes place in two steps: 1) $Co_3O_4 \rightarrow CoO$ (T1), and 2) $CoO \rightarrow Co^0$ (T2). For the unpromoted Co/Ti catalyst, the temperatures of maximum H_2 consumption for the two reduction steps are, respectively, 262 °C (T1) and 443 °C (T2). As observed in the figure, the addition of low amounts of Ru (0.2 wt%) remarkably lowers the temperature for both reduction steps down to 124 °C (T1) and 274 °C (T2). Both T1 and T2 reduction temperatures experience an additional decrease to 100 °C and 226 °C, respectively, with the increase in Ru loading from 0.2 to 0.7 wt%. However, a further increase in Ru content from 0.7 to 1.2 wt% does not produce significant changes in the reduction profile and, hence, in the reducibility of Co_3O_4 and CoO oxides. A small third reduction feature can be perceived at higher temperatures for the CoRu*x*/Ti catalysts (T3= 395-398 °C), which can be ascribed to the reduction of Co^{2+} species displaying a stronger interaction with the TiO_2 support.

Figure S7. EDS elemental mapping for H_2-reduced and passivated Co/Ti (a), CoRu0.1/Ti (b), CoRu0.2/Ti (c), CoRu0.7/Ti (d), and CoRu1.2/Ti (e) catalysts.

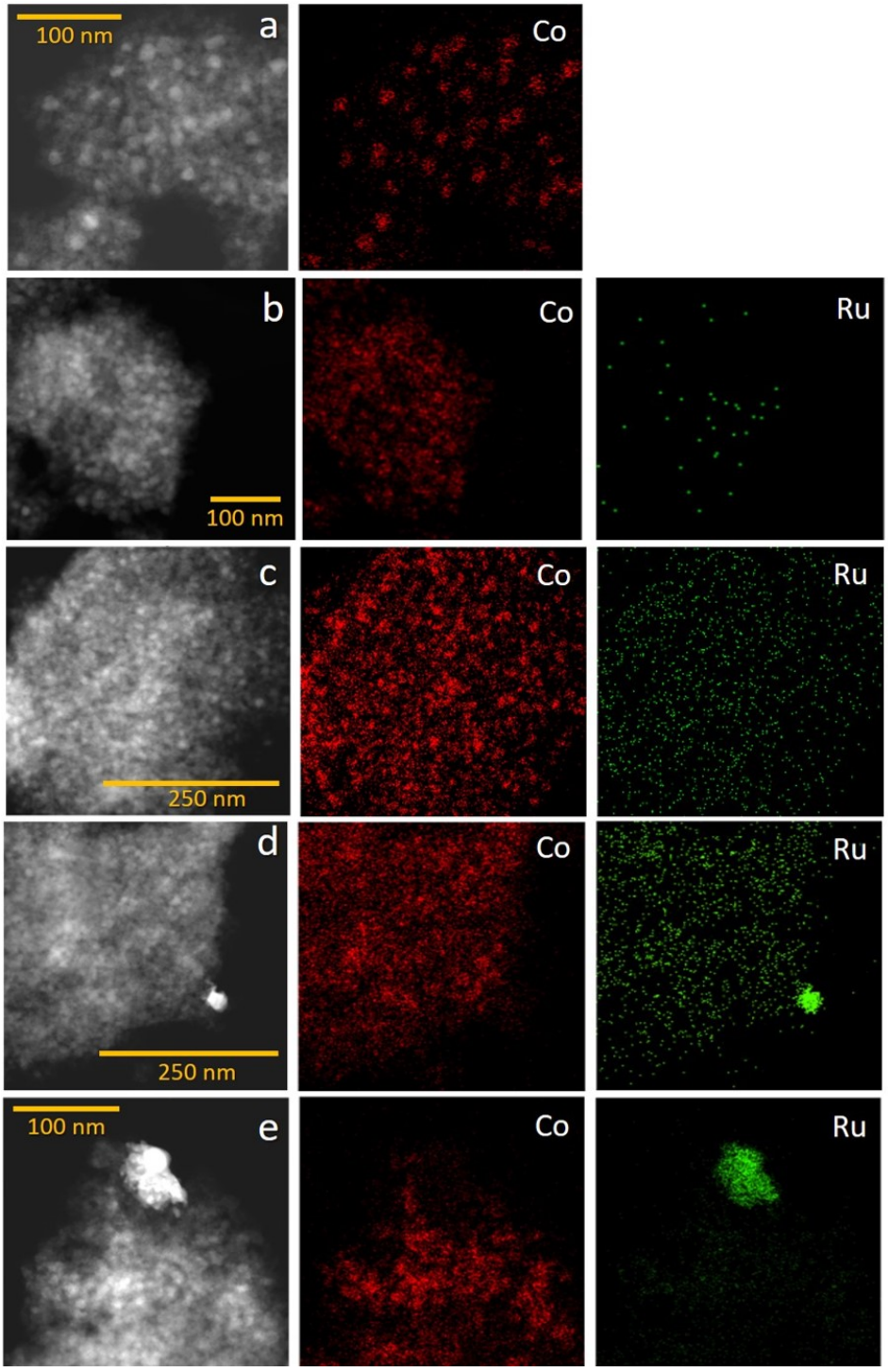

Figure S8. FTIR spectra of CO adsorption recorded at room temperature for as-reduced Co/Ti (a), CoRu0.2/Ti (b), and CoRu1.2/Ti (c). The spectra at CO saturation coverage are shown in blue. Black lines correspond to the background spectra (before CO adsorption). Prior to performing the FTIR-CO experiments, the catalysts were reduced ex situ at 400 °C for 10 h in pure H_2 flow (same conditions as those applied prior FTS) and passivated under flowing diluted O_2. Once loaded in the IR cell, the catalysts were treated again in pure H_2 at 400 °C for 2 h to remove the passivation layer.

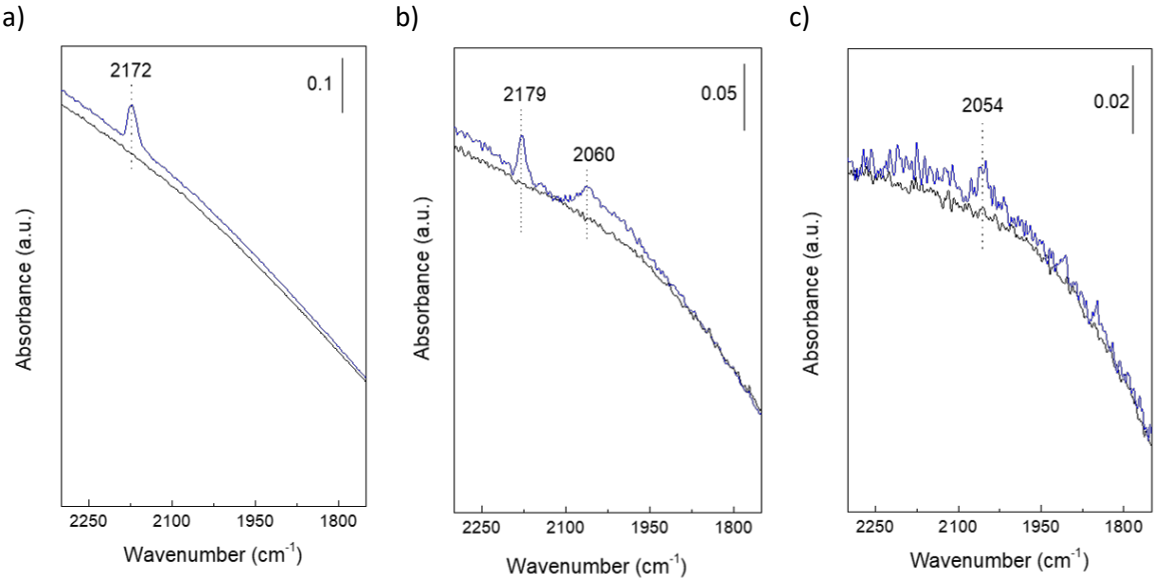

As seen in Figure S8a, a unique IR band at 2172 cm^{-1} related to oxidized Co species [6,7] remaining in the passivated outer layer after the in situ re-reduction treatment in the IR cell is observed in the Co-carbonyl region for Co/Ti. The low concentration of surface Co^0 atoms (below the detection limit at the studied conditions) titrated by CO signs for an extensive SMSI effect in this catalyst after reduction in H_2 at 400 °C, in concur with the H_2 chemisorption results. Differently, an IR band at 2060 cm^{-1} of CO linearly adsorbed on metallic Co is evidenced, besides that of oxidized Co (2179 cm^{-1}), in the IR spectrum of the CoRu0.2/Ti catalyst (Figure S8b), indicating a less pronounced SMSI effect in this catalyst compared to Co/Ti. On the other hand, the remarkably lower intensity of the IR band of CO-Co^0 species at 2054 cm^{-1} in CoRu1.2/Ti (Figure S8c) compared to that in CoRu0.2/Ti is suggestive of a more extended SMSI effect in the former.

Figure S9. Normalized XANES spectra at Ru K-edge for as-reduced CoRu/TiO_2 catalysts with different Ru contents.

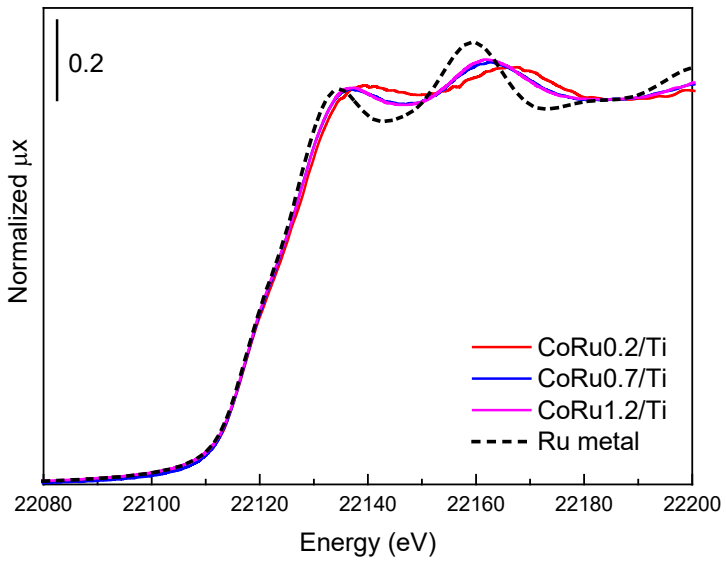

Table S2. Summary of optimized parameters by fitting EXAFS data of catalysts measured at 100 °C after in situ reduction in H_2 and after FTS reaction for 3 h at 220 °C and 1 bar[a].

Sample	Path	N	R (Å)	$\sigma^2_{Ru\text{-}Co}$ (Å^2)	$\sigma^2_{Ru\text{-}Ru}$ (Å^2)	$\Delta E_{0\ Ru\text{-}Co}$ (eV)	$\Delta E_{0\ Ru\text{-}Ru}$ (eV)	R_{factor}
Ru metal	Ru-Ru	12	2.673 ± 0.006	-	0.0030 ± 0.0011	-	5.0 ± 1.2	0.0069
CoRu0.2/Ti	Ru-Co	8.3 ± 0.8	2.498 ± 0.012	0.0076 ± 0.0012	0.0052 ± 0.0006	-1.6 ± 1.6	5.0 ± 0.6	0.0047
	Ru-Ru	1.6 ± 0.5	2.674 ± 0.028					
CoRu0.2/Ti - FTS	Ru-Co	6.9 ± 0.7	2.501 ± 0.012	0.0076 ± 0.0012	0.0052 ± 0.0006	-1.6 ± 1.6	5.0 ± 0.6	0.0055
	Ru-Ru	0.8 ± 0.4	2.711 ± 0.054					
CoRu0.7/Ti	Ru-Co	5.1 ± 0.5	2.504 ± 0.013	0.0076 ± 0.0012	0.0052 ± 0.0006	-1.6 ± 1.6	5.0 ± 0.6	0.0035
	Ru-Ru	4.6 ± 0.4	2.643 ± 0.006					
CoRu1.2/Ti	Ru-Co	4.4 ± 0.4	2.506 ± 0.013	0.0076 ± 0.0012	0.0052 ± 0.0006	-1.6 ± 1.6	5.0 ± 0.6	0.0045
	Ru-Ru	5.8 ± 0.3	2.647 ± 0.005					
CoRu1.2/Ti - FTS	Ru-Co	3.7 ± 0.3	2.514 ± 0.013	0.0076 ± 0.0012	0.0052 ± 0.0006	-1.6 ± 1.6	5.0 ± 0.6	0.0078
	Ru-Ru	4.5 ± 0.3	2.652 ± 0.005					

[a] The fits were performed on the first coordination shell (ΔR = 1.4-3.0 Å) over FT of the $k^1k^2k^3$-weighted χ(k) functions performed in the Δk = 2.6-12.0 Å^{-1} interval, resulting into a number of independent parameters of $2\Delta R\Delta k/\pi$ = 46.5. Non-optimized parameters are recognizable by the absence of the corresponding error bar. S_0^2 = 0.72.

Figure S10. C1s and Ru3d peaks of XPS spectra for as-reduced CoRu0.2/Ti (a), CoRu0.7/Ti (b), and CoRu1.2/Ti (c) catalysts.

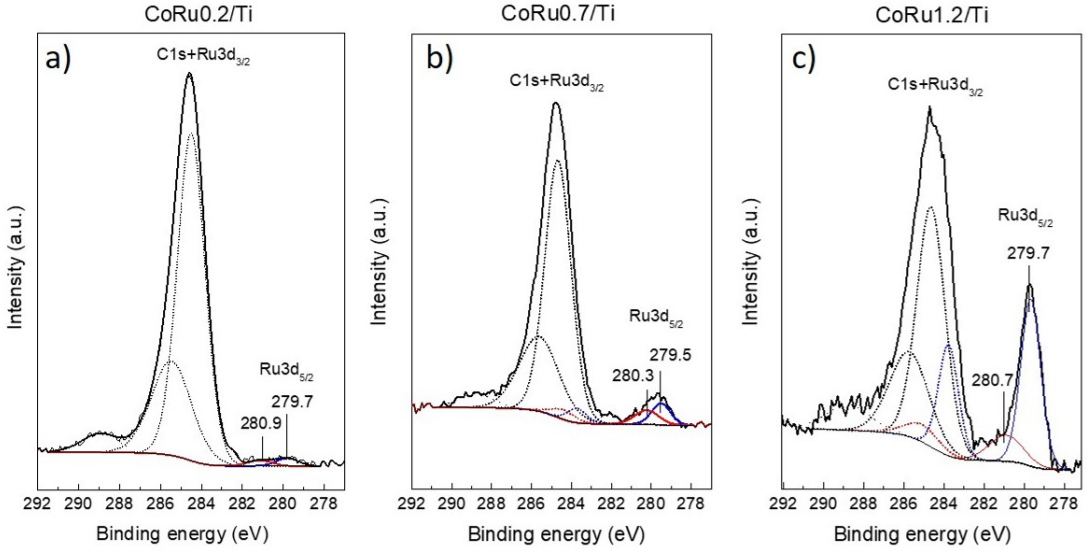

Figure S11. XRD patterns recorded after *in situ* reduction of Co/Ti and CoRu0.2/Ti catalysts in diluted H_2 flow at 400 °C for 3 h. The XRD pattern of the bare TiO_2-anatase support is also shown for an easier identification of the Co-related peaks.

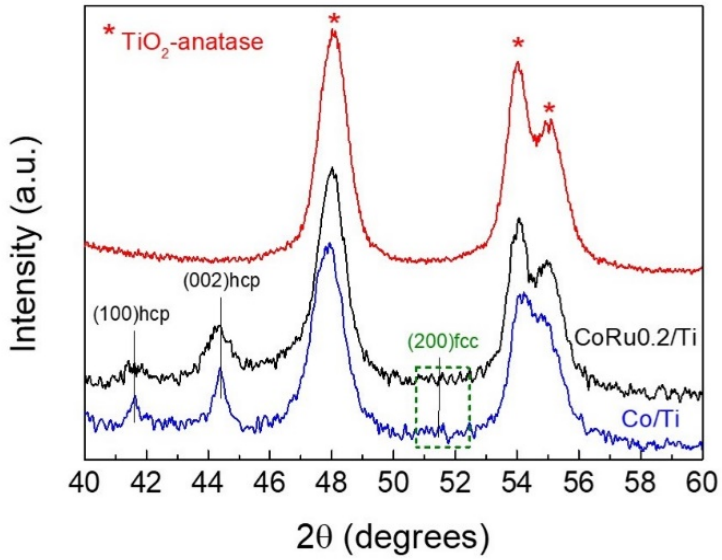

The Co-related diffraction peaks at 2θ = 41.7° and 44.6° are assigned to the (100) and (002) planes of the hcp-Co phase (JCPDS Card No. 05-0727). The presence of these peaks, besides the absence of the peak at $2\theta \sim 51.5°$ related to the (200) plane of fcc-Co (JCPDS Card No. 15-0806), indicates that hcp-Co is the prevailing cobalt crystal phase formed upon reduction in H_2 at 400 °C. The mean Co^0 particle sizes, estimated by line broadening analysis (using the Scherrer equation) of the (002) reflection of hcp-Co (2θ = 44.6°) amounted to 20 nm for the unpromoted Co/Ti sample and to 11 nm for the promoted CoRu0.2/Ti catalyst. This result aligns with the enhanced Co dispersion upon promotion with Ru concluded from the Co particle sizes directly measured by electron microscopy (STEM, Table 1 of manuscript). However, the Co particle sizes estimated by in situ XRD are 1.3 – 1.6 times higher than the sizes obtained by STEM, which can be ascribed to the lower accuracy of the XRD-derived data due to relatively low Co content in our catalysts (~ 12 wt%) resulting in a too low intensity of the Co-related diffractions.

Figure S12. Anderson-Schulz-Flory (ASF) distribution of hydrocarbons obtained in the *pseudo*-steady state for CoRu*x*/Ti catalysts at ca. 10% CO conversion. Reaction conditions: T = 220 °C, P = 20 bar, H_2/CO = 2 mol/mol. The ASF curves have been shifted for the sake of clarity.

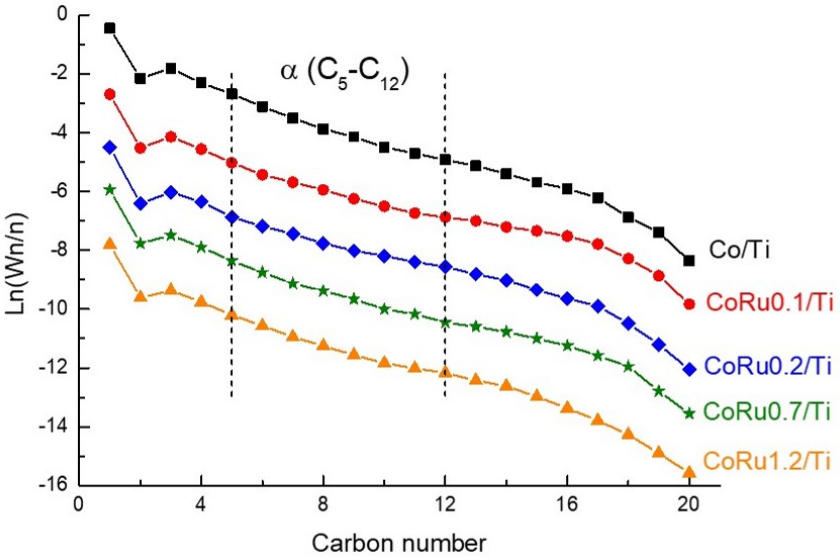

The table below shows the values for the chain growth probability parameter α calculated from the slope of the linear fit of ASF curves in the C_5 to C_{12} range. The statistic R-squared values (R^2) are also given in the table as a measure of the goodness-of-fit.

	Catalyst				
	Co/Ti	CoRu0.1/Ti	CoRu0.2/Ti	CoRu0.7/Ti	CoRu1.2/Ti
α (C_5-C_{12})	0.726	0.768	0.784	0.746	0.753
R^2	0.976	0.988	0.986	0.990	0.978

Figure S13. Influence of Ru loading in the olefin-to-paraffin (O/P) ratio for the C_2-C_4 and C_5-C_8 hydrocarbon fractions at a constant conversion of ca. 10%.

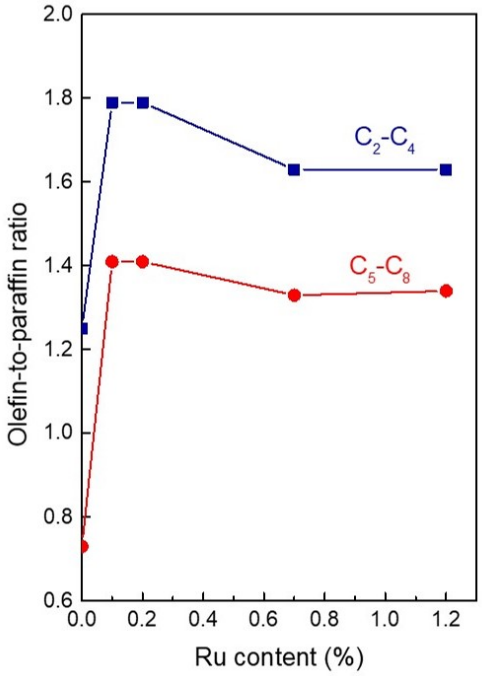

Table S3. Surface density of Co^0 sites (θ_{Co}) and diffusion-related structural parameter (χ) for the Ru-promoted Co/TiO_2 catalysts studied in this work.

Catalyst	$\theta_{Co}\cdot10^{16}$ (Co^0 atoms/m^2)	$\chi\cdot10^{16}$ (m)
CoRu0.1/Ti	19	58
CoRu0.2/Ti	19	53
CoRu0.7/Ti	42	123
CoRu1.2/Ti	34	98

According to the diffusion-controlled selectivity model developed by Iglesia [8], the structural parameter χ was calculated using the following equation:

$$\chi = R_0^2 \cdot \varepsilon \cdot \theta_{Co} / r_p$$

where R_0^2 is the mean radius of catalyst pellets, ε is the fraction of empty pores in the pellet, θ_{Co} is the surface density of metal Co sites per unit area, and r_p is the mean radius of catalyst pores. Since all catalysts have the same pellet size (determined by reactor hydrodynamics) and similar porosity (due to the common TiO_2 support employed in their preparation), differences in the parameter χ among them mainly arise from their distinct surface density of Co^0 sites (θ_{Co}), as shown in Table S3.

Figure S14. Moduli of Fourier transform of k^3-weighted EXAFS spectra (not phase corrected) and fitting curve of CoRu0.2/Ti and CoRu1.2/Ti catalysts in their as-reduced state and after 3 h of FTS reaction at 220 °C and 1 bar.

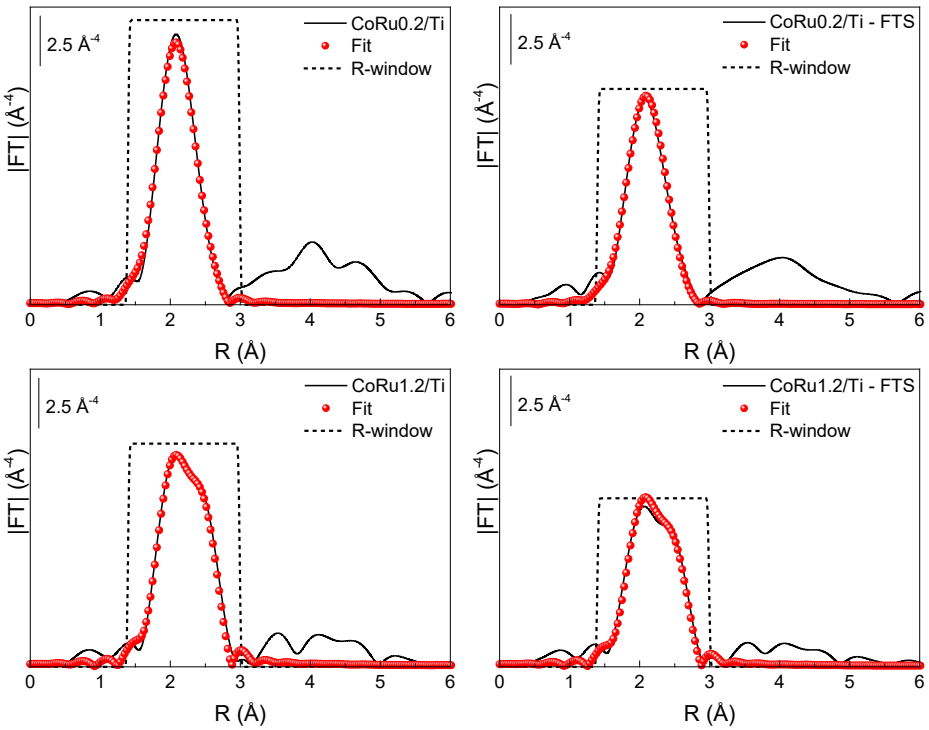

Figure S15. CO-FTIR spectra recorded for Co/Ti (a) and CoRu0.2/Ti (b) catalysts under syngas flow at 9 bar at increasing temperatures: 100 °C (1), 160 °C (2), 220 °C (3), after 2 h at 220 °C (4), and after 4 h at 220 °C (5).

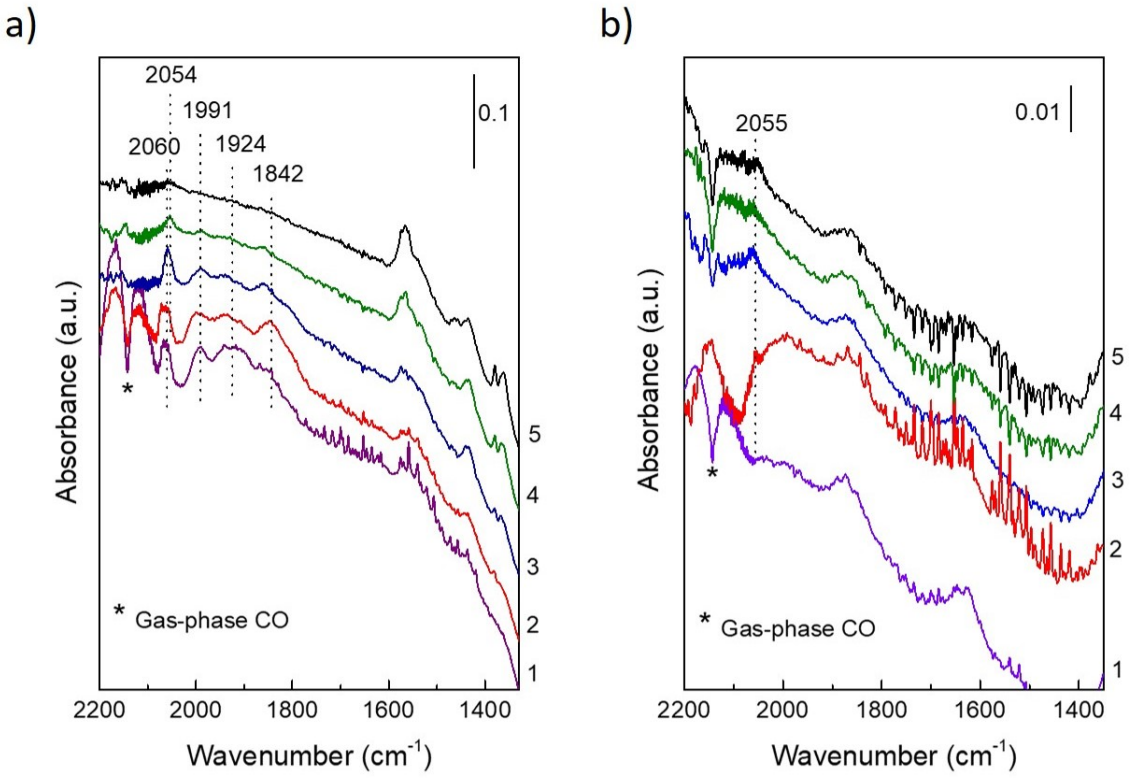

Divergently from the spectra collected for the Co/Ti catalyst at atmospheric pressure (Figure 6c, main text), the cobalt carbonyl band at 2060 cm^{-1} and the bands of cobalt polycarbonyls at 1991, 1924, and 1842 cm^{-1} are readily detected in this sample at 100 °C (Figure S15a, spectrum 1). This signs for an enhanced reactivity at the higher syngas pressure, as anticipated. However, we surprisingly found that the intensity of the IR band at 2060 cm^{-1}, still observed after reaching the reaction temperature of 220 °C (spectrum 3), significantly declined after 2 h of reaction at this temperature (spectrum 4) and completely vanished after reaction with syngas for 4 h (spectrum 5). This can be attributed to the covering of surface Co atoms by adsorbed species. In fact, IR bands of surface intermediate species (1590-1350 cm^{-1} region) were still detected and even increased in intensity during reaction at 220 °C. With respect to the CoRu0.2/Ti catalyst (Figure S15b), a small band at ca. 2055 cm^{-1} could still be observed under FTS conditions (spectra 3-5), although experimental problems related to gas phase subtraction resulted in uncertainties in the accurate identification and position of the IR bands.

Figure S16. $Co2p_{3/2}$ XPS peak (a) and Co LMM Auger peak (b) for the CoRu0.2/Ti catalyst after H_2 reduction (red lines) and after 3 h of reaction with syngas at 220 °C and 1 bar (blue lines). A representative deconvolution of the $Co2p_{3/2}$ XPS peak is shown in panel c) for the H_2-reduced sample.

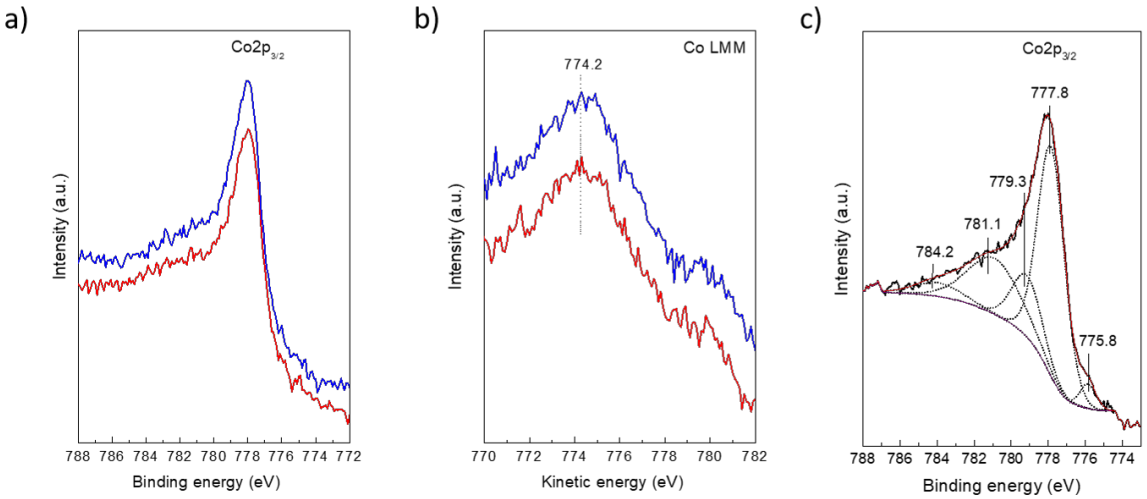

Figure S17. Evolution with time of the mass spectral signal intensity of the product methane (m/z = 15) for CoRu*x*/Ti and Co/Ti catalysts during FTS reaction at 220 °C, 9 bar, and 10 cm^3/min of syngas performed in the HPCR cell connected to the XPS analysis chamber. The MS signals are referenced to that of CO (m/z = 28) and normalized by mass of sample in the pellet.

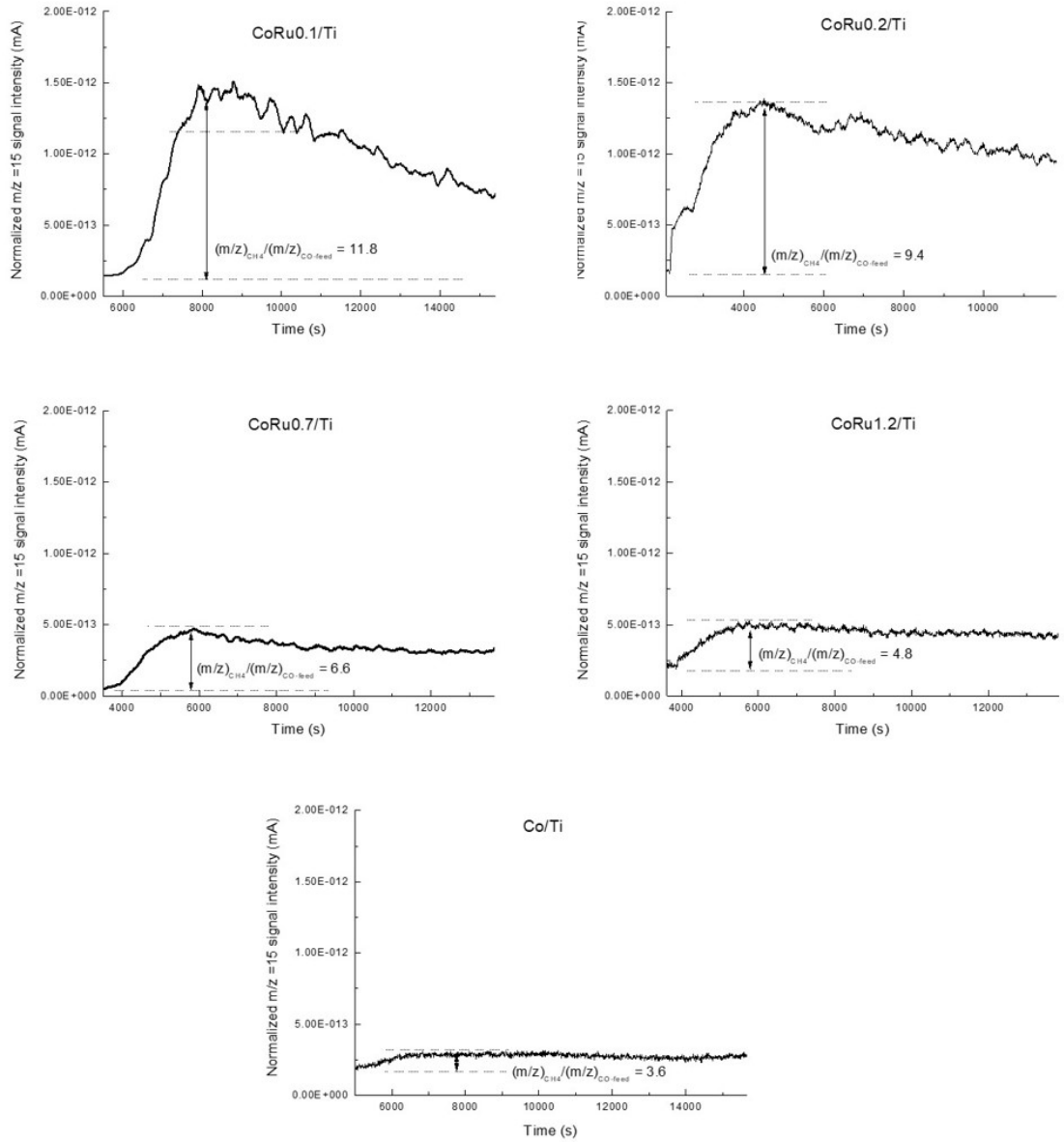

Figure S18. Deconvoluted C1s XPS spectra for the unpromoted and Ru-promoted catalysts after FTS reaction at 200 °C and 9 bar for 3 h.

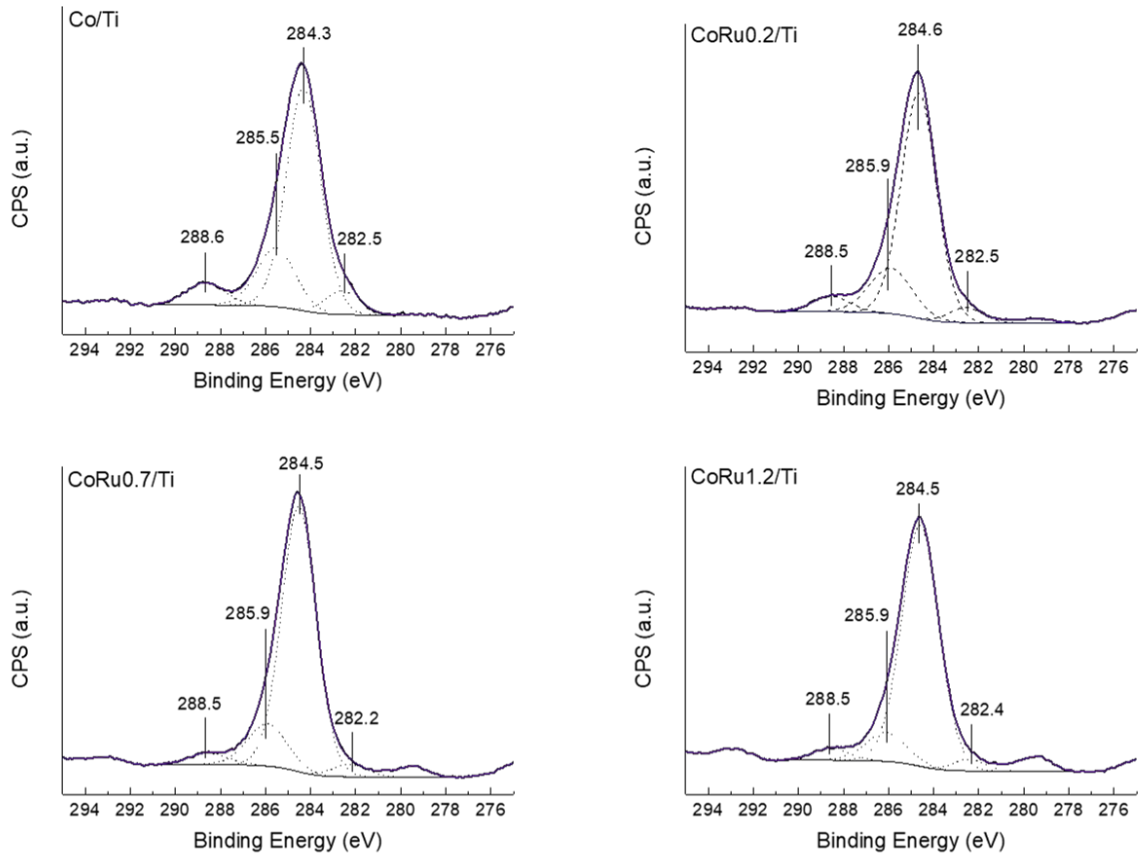

Figure S19. Co2p XPS (panel A) and Co LMM Auger (panel B) spectra of a reference Na-Co/SiO_2 sample after reduction in H_2 (spectra a) and after subsequent carburization with pure CO (spectra b).

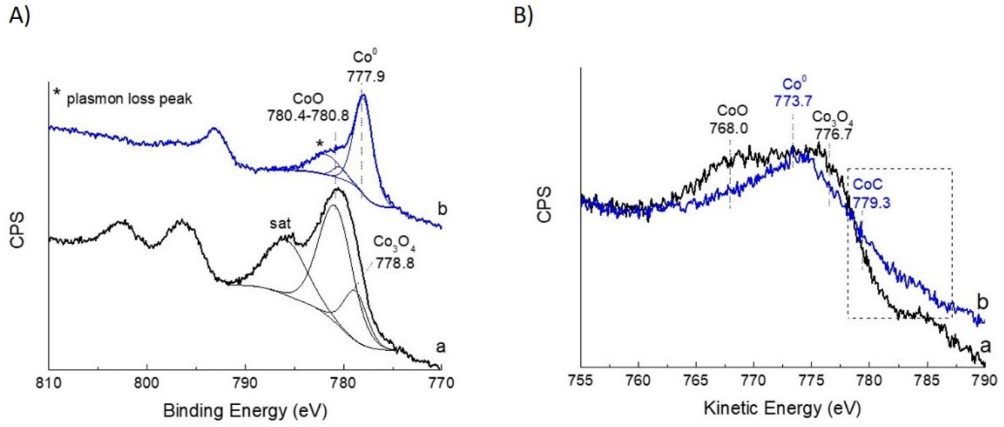

The Co2p XPS spectrum of the H_2-reduced sample (Figure S19A, spectrum a) shows the presence of two components at 780.8 eV (main peak) with a satellite structure at 785.8 eV, characteristic of CoO, and a less intense peak at 778.8 eV related to Co_3O_4. Accordingly, the Co LMM Auger spectrum of the as-reduced sample (Figure S19B, spectrum a) exhibits two main peaks positioned at KE of 776.7 eV and 768.0 eV, yielding α' values of 1555.4 eV and 1548.8 eV which are close to those of CoO and Co_3O_4, respectively, in the Wagner plot (Figure 7b, main text). Therefore, the in situ treatment with H_2 reduced most of the surface Co_3O_4 species originally present in the calcined 1%Na/20%Co-SiO_2 sample (as ascertained by XRD, not shown) to CoO. On the other hand, the Co2p XPS spectrum of the CO-treated sample (Figure S19A, spectrum b) shows a main component at 777.9 eV of Co^0, along with two less intense peaks at higher BE of 780.4 eV and 781.8 eV associated to, respectively, CoO and a plasmon loss peak of metallic cobalt. No signs of a cobalt carbide phase could be evidenced from the Co2p XPS spectrum. However, the Co LMM Auger spectrum of the CO-treated sample (Figure S19B, spectrum b) shows, besides a main peak positioned at KE of 773.7 eV of metallic Co (α' of 1551.6 eV), a shoulder at a higher KE of ca. 779.3 eV (α' of 1557.2 eV), absent in the spectrum of the H_2-reduced sample, that can be assigned to cobalt carbide [9].

Experimental conditions for preparation of sample Na-Co/SiO_2 and XPS-Auger measurements

The 1%Na-20%Co/SiO_2 sample (abbreviated as Na-Co/SiO_2) was prepared as reported in [10]. Briefly, a high-purity grade commercial silica gel (Davisil grade 635, A_{BET} = 480 m^2/g, V_{micro} = 0.75 cm^3/g, mean pore size = 6 nm, particle size = 150-250 µm) was first impregnated to incipient wetness with an aqueous solution containing the required amount of $Co(NO_3)_2 \cdot 6H_2O$ to achieve a nominal Co content

of 20 wt%. After drying at 80 °C overnight, 1.0 wt% Na was introduced via incipient wetness impregnation of Co/SiO_2 with an aqueous solution of Na_2CO_3 (99.5%, Sigma Aldrich), followed by drying at 80 °C overnight and calcination in air (450 mL/(min·g)) at 300 °C for 3 with ramping of 1 °C/min.

For XPS-Auger measurements, about 10 mg of the calcined sample were mounted in the sample holder located in a high-pressure catalytic reactor (HPCR) connected to the XPS analysis chamber. The sample was then reduced in situ with pure H_2 (5 mL/min) at 400 °C for 4 h with a ramping of 5 °C/min, and the Co2p XPS and Co LMM Auger spectra recorded. Subsequently, the H_2-treated sample was submitted to an in situ carburization treatment under flowing pure CO (10 mL/min) at 290 °C and 3.5 bar for 5 h, and the Co2p XPS and Co LMM Auger spectra recorded again.

References

[1] Reuel, R. C.; Bartholomew, C. H., Effects of support and dispersion on the CO hydrogenation activity/selectivity properties of cobalt. *Journal of Catalysis* **1984**, 85 (1), 78-99.

[2] Shen, X.; Garces, L.-J.; Ding, Y.; Laubernds, K.; Zerger, R. P.; Aindow, M.; Neth, E. J.; Suib, S. L., Behavior of H_2 chemisorption on Ru/TiO_2 surface and its application in evaluation of Ru particle sizes compared with TEM and XRD analyses. *Applied Catalysis A: General* **2008,** *335* (2), 187-195.

[3] Bertella, F.; Concepción, P.; Martínez, A., The impact of support surface area on the SMSI decoration effect and catalytic performance for Fischer-Tropsch synthesis of $Co\text{-}Ru/TiO_2$-anatase catalysts. *Catalysis Today* **2017,** *296*, 170-180.

[4] Eschemann, T. O.; Oenema, J.; de Jong, K. P., Effects of noble metal promotion for Co/TiO_2 Fischer-Tropsch catalysts. *Catalysis Today* **2016,** *261*, 60-66.

[5] Hong, J.; Marceau, E.; Khodakov, A. Y.; Gaberová, L.; Griboval-Constant, A.; Girardon, J.-S.; Fontaine, C. L.; Briois, V., Speciation of Ruthenium as a Reduction Promoter of Silica-Supported Co Catalysts: A Time-Resolved in Situ XAS Investigation. *ACS Catalysis* **2015,** *5* (2), 1273-1282.

[6] Rygh, L. E. S.; Ellestad, O. H.; Klæboe, P.; Nielsen, C. J., Infrared study of CO adsorbed on $Co/\gamma\text{-}Al_2O_3$ based Fischer-Tropsch catalysts; semi-empirical calculations as a tool for vibrational assignments. *Phys. Chem. Chem. Phys.* **2000,** *2* (8), 1835-1846.

[7] Kadinov, G.; Bonev, C.; Todorova, S.; Palazov, A., IR spectroscopy study of CO adsorption and of the interaction between CO and hydrogen on alumina-supported cobalt. *J. Chem. Soc., Faraday Trans.* **1998,** *94* (19), 3027-3031.

[8] E. Iglesia, Design, synthesis, and use of cobalt-based Fischer-Tropsch synthesis catalysts. *Applied Catalysis A: General* **1997**, 161, 59-78.

[9] Ye, D. X.; Pimanpang, S.; Jezewski, C.; Tang, F.; Senkevich, J. J.; Wang, G. C.; Lu, T. M., Low temperature chemical vapor deposition of Co thin films from $Co_2(CO)_8$. *Thin Solid Films* **2005,** *485* (1-2), 95-100.

[10] Gnanamani, M. K.; Jacobs, G.; Keogh, R. A.; Shafer, W. D.; Sparks, D. E.; Hopps, S. D.; Thomas, G. A.; Davis, B. H., Fischer-Tropsch synthesis: Effect of pretreatment conditions of cobalt on activity and selectivity for hydrogenation of carbon dioxide. *Applied Catalysis A: General* **2015,** *499*, 39-46.